iScience

CellPress
OPEN ACCESS

Article

Contribution of septins to human platelet structure and function

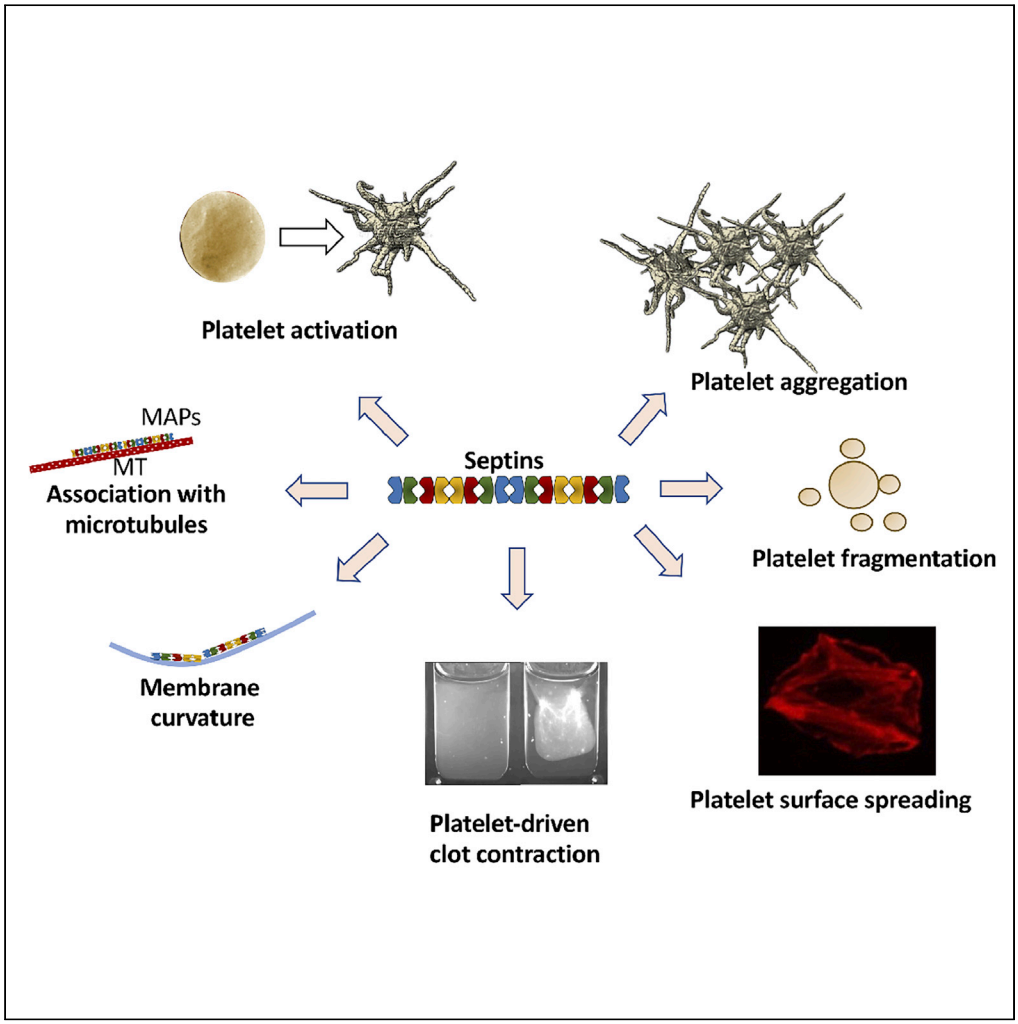

Oleg V. Kim, Rustem I. Litvinov, Elmira R. Mordakhanova, Erfei Bi, Olga Vagin, John W. Weisel

olegkim@pennmedicine.upenn.edu (O.V.K.)
weisel@pennmedicine.upenn.edu (J.W.W.)

Highlights

Septin-2 and Septin-9 localize at platelet periphery together with microtubules

Platelet activation causes spatial rearrangement and clustering of septins

Septins contribute to platelet morphology and expression of activation markers

Septin assembly supports platelet biomechanics including spreading and contraction

Kim et al., iScience *25*, 104654
July 15, 2022
https://doi.org/10.1016/j.isci.2022.104654

iScience

CellPress
OPEN ACCESS

Article

Contribution of septins to human platelet structure and function

Oleg V. Kim,[1,*] Rustem I. Litvinov,[1] Elmira R. Mordakhanova,[2] Erfei Bi,[1] Olga Vagin,[3,4] and John W. Weisel[1,5,*]

SUMMARY

Although septins have been well-studied in nucleated cells, their role in anucleate blood platelets remains obscure. Here, we elucidate the contribution of septins to human platelet structure and functionality. We show that Septin-2 and Septin-9 are predominantly distributed at the periphery of resting platelets and co-localize strongly with microtubules. Activation of platelets by thrombin causes clustering of septins and impairs their association with microtubules. Inhibition of septin dynamics with forchlorfenuron (FCF) reduces thrombin-induced densification of septins and lessens their colocalization with microtubules in resting and activated platelets. Exposure to FCF alters platelet shape, suggesting that septins stabilize platelet cytoskeleton. FCF suppresses platelet integrin αIIbβ3 activation, promotes phosphatidylserine exposure on activated platelets, and induces P-selectin expression on resting platelets, suggesting septin involvement in these processes. Inhibition of septin dynamics substantially reduces platelet contractility and abrogates their spreading on fibrinogen-coated surfaces. Overall, septins strongly contribute to platelet structure, activation and biomechanics.

INTRODUCTION

Septins are a family of GTP-binding cytoskeletal proteins originally identified in yeast as essential for cytokinesis and morphological changes (Oh and Bi, 2011). In mammalian cells, 13 septins have been identified (SEPTIN1-SEPTIN12 and SEPTIN14), which are classified in four subgroups according to their sequence similarity and named after their prominent members: SEPTIN2, 3, 6, and 7 (Kinoshita, 2003). Previous studies have shown that the simplest hetero-oligomeric complex of septins comprises either six or eight subunits from three or four different subgroups, respectively, incorporating two copies of each subunit (McMurray and Thorner, 2019; Mendonça et al., 2019) (Figure 1). Although septins are widely expressed in human tissues (Hall et al., 2005), some septins (SEPTIN2,4,7,8,9, and 10) have ubiquitous distribution, whereas others were found to be tissue-specific (Hall et al., 2005; Zuvanov et al., 2019). Septin protein subunits are known to self-associate, forming nonpolar rod-like oligomers and higher-order polymeric structures in yeast and mammalian cells (McMurray and Thorner, 2019). The septin rod-like oligomers form short filaments that further assemble into bundles, rings, gauzes, and sheet-like structures (McMurray and Thorner, 2019; Mendonça et al., 2019). Septins form a scaffold, mediating the association and/or organization of many proteins or cellular structures including the cytoskeletal components, such as microtubules and actin, with cell membranes (Bridges and Gladfelter, 2015; Dolat et al., 2014b; Mostowy and Cossart, 2012). In nucleated cells septins were found to mediate a variety of functions, including cytokinesis, sperm motility, autophagy, exocytosis, cell migration and matrix adhesion (Dolat et al., 2014b; Ihara et al., 2005; Longtine et al., 1996; Mostowy et al., 2010; Tokhtaeva et al., 2015; Verdier-Pinard et al., 2017). Septins can affect branching, elongation, and receptor-membrane association of the cytoskeleton, as shown in axons and during invasion of Listeria into host cells (Hu et al., 2012; Mostowy et al., 2011). Septins were shown to play a role in inflammation by regulating pathogen uptake by phagocytes, controlling immune cell infiltration, regulating tissue barrier permeability, and contributing to post-inflammatory tissue fibrosis (Ivanov et al., 2021).

Platelets are cytoplasmic fragments of megakaryocytes, polyploid cells residing in the bone marrow and lungs (Junt et al., 2007; Lefrançais et al., 2017). Platelets are the smallest anucleate blood cells, 2–4 μm in size that play a pivotal role in hemostasis and thrombosis. Their main function is to prevent blood loss by forming sticky platelet aggregates (a hemostatic plug) at the site of vascular injury (Brass et al., 2017;

[1]Department of Cell and Developmental Biology, Perelman School of Medicine, University of Pennsylvania, Philadelphia, PA, USA

[2]Institute of Fundamental Medicine and Biology, Kazan Federal University, Kazan, Russian Federation

[3]Department of Pediatrics, Geffen School of Medicine at UCLA, Los Angeles, CA, USA

[4]Veterans Affairs Greater Los Angeles Health Care System, Los Angeles, CA, USA

[5]Lead contact

*Correspondence: olegkim@pennmedicine.upenn.edu (O.V.K.), weisel@pennmedicine.upenn.edu (J.W.W.)

https://doi.org/10.1016/j.isci.2022.104654

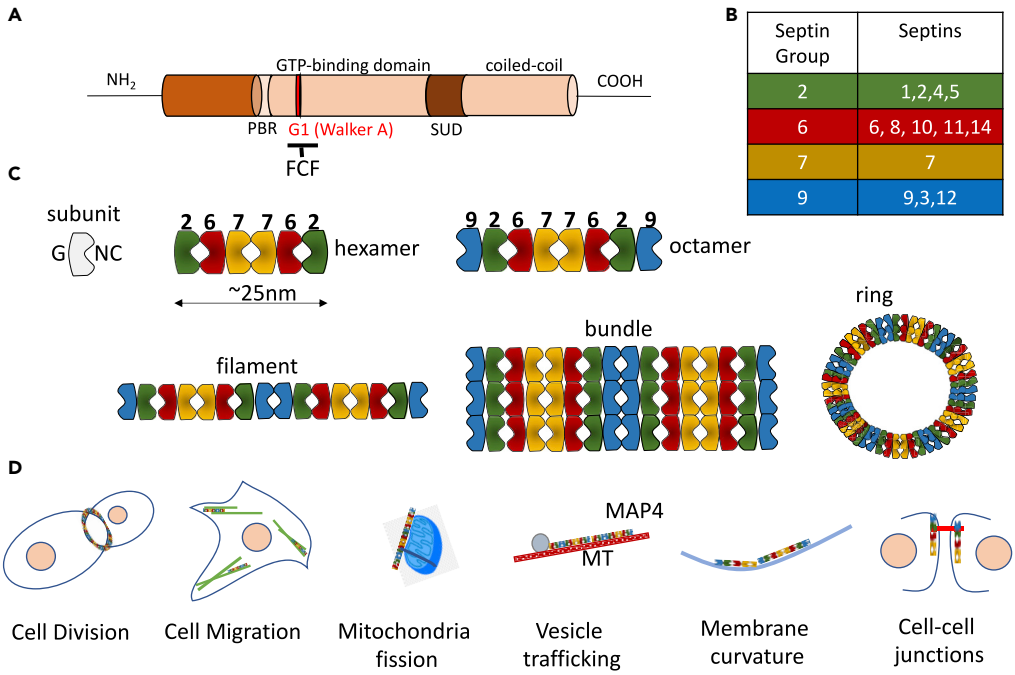

Figure 1. Schematic representation of the organization of septins and their involvement in cell functions

(A) Septin domain structure comprises a GTP-binding domain, a phosphoinositide-binding polybasic region (PBR), a septin unique domain (SUD), and one or several coiled-coil domains (Cavini et al., 2021). The lengths of N- and C- terminus vary among different septins(Trimble, 1999). Septin inhibitor, forchlorfenuron (FCF), interacts with the Walker A motif, preventing septin binding and hydrolysis (Angelis et al., 2014).

(B) Septin homology-based subgoups. Septins are classified into four distinct subgroups based on amino acid sequence similarity (Kinoshita, 2003).

(C) Canonical heterooligomeric complexes of septins formed by alternate G-G and N-C interfaces and septins higher order structures (Sirajuddin et al., 2009).

(D) The most well defined involvements of septins in cellular functions (Dolat et al., 2014a; Ivanov et al., 2021).

Rosen et al., 2001). The initial interaction of platelets with the exposed sub-endothelium at a vessel injury site is mediated by the receptor glycoproteins GPIb-IX-V, GPVI, GPIa/IIa (integrin α2β1) followed by intracellular signaling that promotes platelet adhesion and aggregation. Platelet activation is accompanied by an increase of cytosolic [Ca^{2+}], secretion of intracellular granule content, cytoskeletal remodeling, and transition of the integrin αIIbβ3 on the platelet surface from the inactive to active state capable of interacting with extracellular ligands, such as fibrinogen and fibrin (Scharf, 2018; Shattil, 1999, 2005). Activated platelets expose phosphatidylserines (PS), anionic phospholipids, mediating assembly of the enzymatic complexes that catalyze thrombin generation on or near the platelet surface (Monroe Dougald et al., 2002). Thrombin not only causes activation of circulating platelets but also catalyzes conversion of fibrinogen into fibrin, resulting in formation of a polymeric network that stabilizes a blood clot or thrombus (Weisel, 2007). Platelet activation is accompanied by translocation of adhesive P-selectin from intracellular α-granules to the plasma membrane, allowing for platelet rolling over endothelial cells and platelet-leukocyte aggregation (Frenette et al., 1995; Merten and Perumal, 2000; Yokoyama et al., 2005). Besides supporting the blood clotting enzymatic cascade, activated platelets drive contraction or volume shrinkage of a blood clot by pulling on fibrin fibers (Kim et al., 2017) that is an important pro- and antithrombotic mechanism (Evtugina et al., 2020; Le Minh et al., 2018; Tutwiler et al., 2017).

Several septins (SEPTIN2, 4, 5, 6, 7, 8, 9, and 11) have been identified in human platelets, with the intraplatelet distribution and function being studied for Septins-4, -5, -6 and -8. The relative abundance of septin proteins in human platelets according to (Kim et al., 2014; Pinto et al., 2014) is the following: Septin-7>Septin-11>Septin-2>Septin-5>Septin-6>Septin-9. Confocal microscopy of Septins-5 and -6 in human platelets showed that they self-organize in higher-order ring-like structures (Martinez et al., 2006). Human platelet Septin-4 was shown to interact with Septin-8 (Bläser et al., 2004) whereas Septin-5 formed a complex with Septins-6, -7, and -9 (Martinez et al., 2006). Septin-5 was localized to the areas surrounding human platelet storage-granules (Dent et al.,

2002) and formed a complex with syntaxin 4, a protein involved in platelet secretion. Septins-4 and -8 were found to surround α-granules in human resting platelets and translocate toward platelet periphery upon platelet activation, suggesting the involvement of septins in platelet granule transport and exocytosis (Bläser et al., 2004). Involvement of septins in platelet functions has been studied in mouse models. In particular, deletion of Septin-5 in a mouse caused platelet aggregation and release of serotonin under the action of subthreshold concentrations of collagen (Dent et al., 2002). Platelets from Septin-8 knock-out mice displayed impaired activation of the αIIbβ3 integrin, α-granule exocytosis, αIIbβ3-mediated platelet aggregation and spreading as well as reduced thrombin generation (Neubauer et al., 2021).

Although it is increasingly evident that septins are an important component of the platelet cytoskeleton, the role of septins in human platelet biology, i.e. platelet production and fate, structure, and function, remains largely unknown. In this study, we focused on Septin-2 and Septin-9 because of their involvement in a relatively broad range of cellular functions compared to other septins (Beites et al., 2001; Ihara et al., 2005; Nakahira et al., 2010; Pagliuso et al., 2016; Spiliotis and Nelson, 2006; Sun et al., 2020). Both Septin-2 and Septin-9 are involved in exocytosis, intracellular trafficking, vesicle transport, cytoskeleton organization (Beites et al., 2001; Ihara et al., 2005; Nakahira et al., 2010; Spiliotis and Nelson, 2006). In addition, Septin-2 is involved in mitochondrial fission, neuronal differentiation and growth (Pagliuso et al., 2016; Tada et al., 2007). Septin-9 participates in cytokinesis; it has also been associated with a variety of human diseases, including the development of malignant tumors (El Amine et al., 2013; Sun et al., 2020). Also, Septin-2 and Septin-9 belong to the most and least abundant septins that are present in human platelets and plasma (see Table S1).

We used a combination of high-resolution confocal microscopy and a variety of platelet functional assays to elucidate the contribution of human septins to platelet structure and function. Our results reveal that in resting platelets Septin-2 and Septin-9 localize in closeness, proximity to the microtubule marginal ring. Activation of platelets with thrombin decreases colocalization of Septins-2 and -9 with microtubules and causes septin clustering. Inhibition of septin assembly with a septin inhibitor, forchlorfenuron (FCF) (Hu et al., 2008; Iwase et al., 2004), disturbs septin organization in resting and activated platelets. Importantly, the impairment of septin assembly with FCF alters the membrane expression of platelet activation markers, including phosphatidylserine, active αIIbβ3 integrin, and P-selectin. Moreover, FCF significantly affects spreading of platelets on a fibrinogen-coated surface and their contractility, suggesting that septin dynamics is important for platelet biomechanics.

RESULTS

Intracellular distribution of Septin-2 and Septin-9 and their association with microtubules in resting platelets

To gain insights into the role of septins in platelet structure and function, we first analyzed the distribution of septins within resting unstimulated platelets and established the spatial relations of septins with microtubules. Organization of the platelet cytoskeletal proteins was studied after immunofluorescent staining of Septin-2 and Septin-9 as well as α-tubulin of microtubules. Analysis of confocal microscopy z stack images of individual resting platelets revealed remarkable distinctions in the location and density of Septin-2 and Septin-9. The majority of the platelet Septin-2 was concentrated at the cell periphery, forming a spotted circular structure (microscopic ring), while Septin-9 formed clusters at the platelet periphery as well as in the internal parts of the cells (Figures 2A, 2C, S1 and Complementary results, Analysis of colocalization between Septin-2 and Septin-9 in resting platelets). Because human platelets contain circumferential subcortical microtubules, we analyzed colocalization of Septin-2 and Septin-9 with α-tubulin based on the fluorescence intensity correlation and co-occurrence (spatial overlap) of the corresponding pair of fluorophores (see STAR Methods, section protein colocalization analysis). The difference between the co-occurrence and correlation is that the co-occurrence measures the extent of the spatial overlap between two fluorescent probes whereas the correlation evaluates the relationship between the fluorescence intensities in the corresponding pixels comprising the images of the two fluorophores (Aaron et al., 2018).

The mean Pearson's correlation coefficient (PCC) of fluorescence intensities between Septin-2 or Septin-9 and α-tubulin showed that both Septin-2 (SPT2) and Septin-9 (SPT9) were associated strongly with α-tubulin (αT) in the subcortical marginal band (MB) at the periphery of resting platelets (Figures 2B and 2D): average $PCC^{SPT2/\alpha T}{}_{MB}$ = 0.82, $PCC^{SPT9/\alpha T}{}_{MB}$ = 0.82 (the numbers are statistically significant with respect to the random overlap by Costes' method) (Costes et al., 2004). In contrast to the peripherally distributed septins,

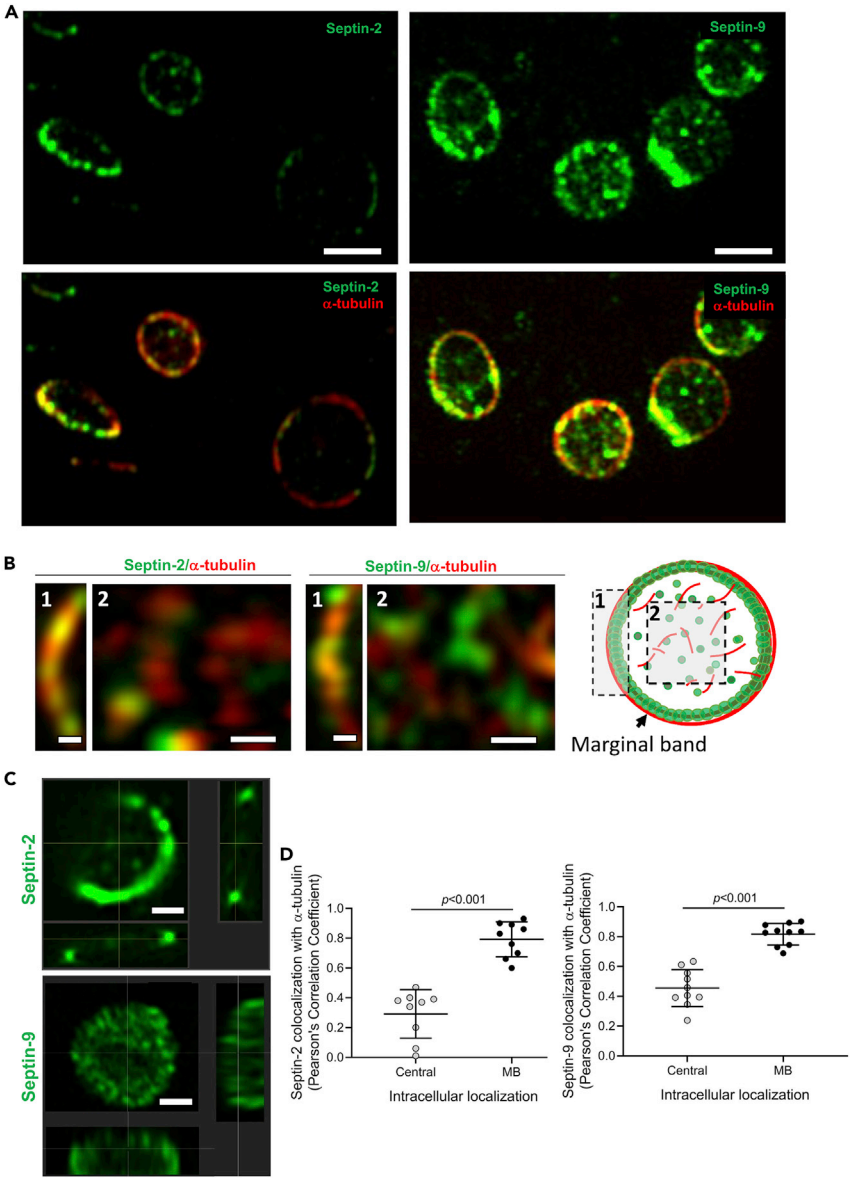

Figure 2. Differential distribution of Septin-2 and Septin-9 within resting platelets and their colocalization with microtubules

(A) Confocal microscopy of unstimulated platelets immunostained for Septin-2, Septin-9, and α-tubulin. Septin-2 forms a ring-like circular structure strongly co-localized with the microtubule marginal band. Septin-9 is located both in the central part and cell periphery where it is co-localized with α-tubulin. Scale bar = 1 μm. The images are the projections of optical z stack slices.

(B) Zoomed-in views of co-stained Septin-2/α-tubulin and Septin-9/α-tubulin (B left) at the platelet peripheral marginal band (MB, "1") and central compartment (Central, "2") regions, schematically illustrated in (B right).

(C) Spatial distributions of Septin-2 and Septin-9 in a single platelet shown in orthogonal cross-sections of a reconstructed 3D image. Scale bar = 0.6 μm.

(D) Quantification of the degree of colocalization between Septin-2 and α-tubulin and Septin-9 and α-tubulin for the platelet peripheral marginal band and the central part, schematically illustrated in (B).

The fluorescence correlation between Septin-2, Septin-9 and α-tubulin shown as Pearson's correlation coefficient (PCC) (D).

The results are presented as a median and IQR; significance tested by the Wilcoxon matched-pairs signed rank test.

Table 1. Summary of the structural and functional roles of septins in resting and activated human platelets revealed in this study

Findings	Implications
In resting and thrombin-activated platelets, Septin-2 and -9 are preferentially located at the cell periphery, **colocalizing with α-tubulin**, with minor punctate distribution in the central region.	Septins may be associated with microtubules in resting platelets via different molecular linkers (such as MAP4).
In resting and thrombin-activated platelets, **FCF decreases colocalization** of both septins with α-tubulin. FCF at ≤50 μM has no effect on the intraplatelet ATP content.	FCF alters septin localization in platelets with no effect on energy metabolism and, hence, can be used as a tool to assess septin function in platelets.
FCF induces changes in the **morphology of resting platelets**, including cell elongation and formation of membrane protrusions	Septins play a role in stabilizing the platelet discoid shape and curved plasma membrane.
In thrombin-activated platelets, Septin-2 and -9 form intense fluorescent **clusters**, which is **prevented by FCF**.	Reorganization of septins may be involved in structural changes in response to platelet activation.
In thrombin-activated platelets, **colocalization** between both septins and α-tubulin is **reduced**. FCF does not prevent the effect.	Structural reorganization of septins during platelet activation dissociate them from tubulins.
Fragmentation of thrombin-activated platelets in PRP-clots is enhanced by pre-treatment of resting platelets with FCF.	Septins contribute to the structural integrity of activated platelets.
During **spreading of resting platelets** on fibrinogen-coated surfaces, the Septin-2 ring structure disintegrate into filament- and puncta-like forms. FCF prevents this effect and abrogates the ability of platelets to spread and form actin stress fibers.	Septin dynamics are involved in cytoskeletal rearrangements underlying the development of lamellipodia and cell spreading.
In resting platelets, FCF increases the **surface expression of P-selectin**	Septins are involved in secretion of proteins from platelet α-granules
Pre-treatment of resting platelets with FCF increases **surface exposure of phosphatidylserine** in stimulated platelets.	Septin dynamics are involved in regulation of the membrane asymmetry of phospholipids in platelets.
Pre-treatment of resting platelets with FCF reduces the **αIIbβ3 integrin activation** in stimulated platelets and impairs their aggregation	Septins promote activation of integrin αIIbβ3, increasing their adhesiveness and ability to aggregate
Pre-treatment of resting platelets with FCF impairs **contraction of clots** induced by adding thrombin to platelet-rich plasma.	Septins are involved in platelet contractile force generation and/or force mechanotrunsduction to the extracellular fibrin matrix

Septin-2 and Septin-9 located in the platelet central domains both displayed significantly lower fluorescence correlation with α-tubulin (Figures 2B and 2D): average $PCC^{SPT2/\alpha T}_{Central}$ = 0.32, $PCC^{SPT9/\alpha T}_{Central}$ = 0.46, Costes p-values > 0.95, $p < 0.001$. As an independent confirmation, quantification of the co-occurrence of septins with α-tubulin in terms of the mean Mander's colocalization coefficient (MCC) (STAR Methods, section protein colocalization analysis) revealed strong spatial overlap of both Septin-2 and Septin-9 with the microtubule band (MB) and their decreased overlap in central parts of resting platelets (Complentary results, Analysis of co-occurrence between Septin-2,9 and α-tubulin for resting and activated platelets and S2A.) Therefore, the high PCC and MCC values for Septin-2, Septin-9 and α-tubulin for the platelet marginal band suggest a strong association between septins and the subcortical microtubules. At the same time, the reduced PCC and MCC values for septins and α-tubulin in the central parts of platelets indicate poor colocalization and random and largely unrelated spatial organization of the proteins, despite their presence in the cell center in detectable amounts.

Thus, in resting platelets, Septin-2 and -9 are preferentially located at the cell periphery, co-localizing with α-tubulin, with minor punctate distribution in the central region (see also Table 1). Of note, the septins studied reveled strong colocalization with the membrane structure at the periphery and weak colocalization within the internal portions of platelets, supporting the idea that the septins are likely to associate more with the microtubule peripheral ring than with the plasma membrane (Figure S3). In addition, co-precipitation of Septin-2 and α-tubulin suggests their direct interaction or a close association (Figure S4).

Changes in the intracellular distribution of Septin-2 and Septin-9 and their association with microtubules in thrombin-activated platelets

Platelets treated with thrombin displayed dramatic intracellular rearrangement of septins as compared to septin organization in resting cells. First, in thrombin-activated platelets both Septin-2 and Septin-9 formed intense fluorescent clusters (Figures 3A and 3B), indicating condensation/densification of the proteins in response to platelet stimulation. To quantify the degree of compaction of septins, the corresponding

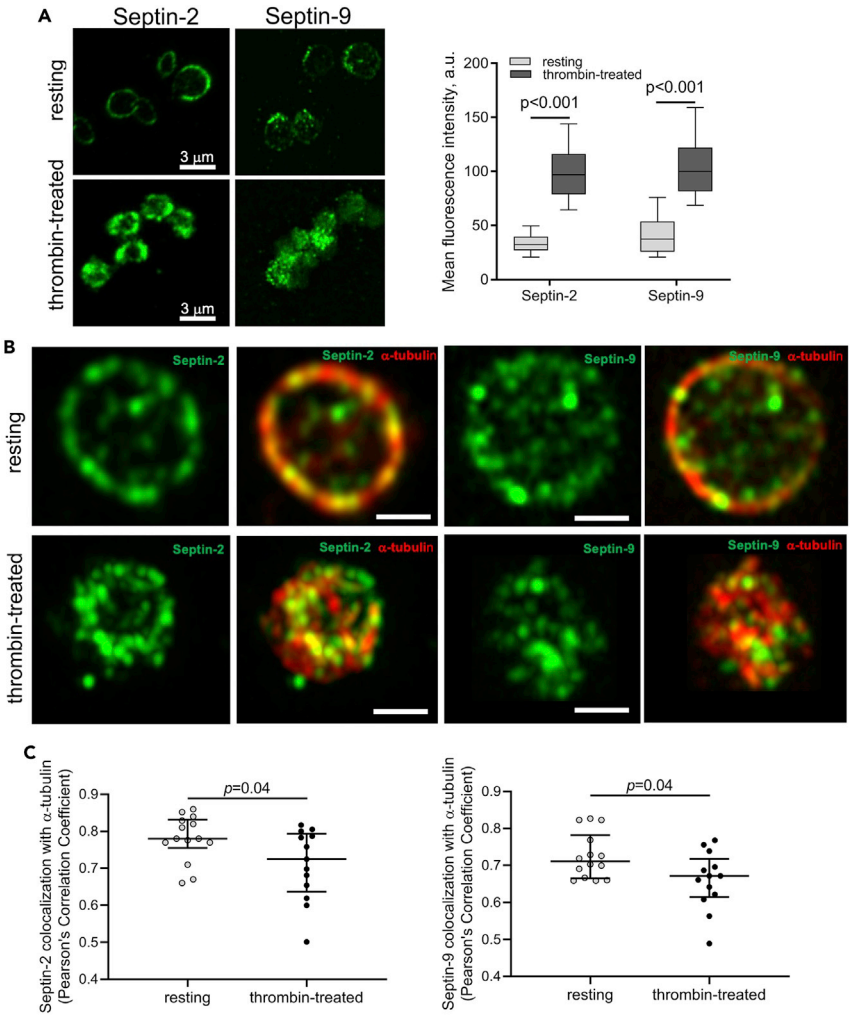

Figure 3. Redistribution of Septin-2 and Septin-9 in platelets upon thrombin-induced activation

(A, left) Confocal microscopy of platelets stained for Septin-2 and Septin-9 in resting and thrombin-treated platelets. Scale bar = 3 μm. (A, right) Mean fluorescence intensity of a whole cell for Septin-2 (n = 110) and Septin-9 (n = 110) measured at the identical settings of a confocal fluorescent microscope, computed as the mean intensity value of all the non-background signal. A two-tailed Mann-Whitney U test.

(B) Distributions of Septin-2, Septin-9 and α-tubulin in a platelet before (top row) and after (bottom row) treatment of platelets with thrombin. Scale bar = 1 μm. Projections of optical z stack slices.

(C) Changes in colocalization between Septin-2 and tubulin in resting and thrombin-activated platelets.

Quantification of colocalization between Septin-2, Septin-9 and α-tubulin based on the fluorescence intensity correlation analysis and presented in terms of Pearson correlation coefficients (PCC).

The results are presented as a median and IQR. Significance tested by the Mann-Whitney U-test.

septin-related fluorescence intensities measured at identical microscope settings were compared in resting and thrombin-activated platelets. Platelet stimulation with thrombin caused a ~2-fold increase in the average fluorescence intensity of Septin-2 and Septin-9 (Figures 3A and S5), suggesting polymerization, aggregation or other type of densification of platelet septins. Of note, there was a significant increase in Septin-2 protein synthesis following platelet activation (Figure S6). In addition, septin compaction was assessed by evaluating the area of septins in z stack images of resting and activated platelets, revealing about a 30–38% decrease in the septin-occupied area within platelets upon activation (Figure S7).

Second, septins changed their intracellular localization and the degree of association with microtubules, so that the Septin-2 clusters were accumulated almost exclusively at the cell periphery whereas the Septin-9 clusters were seen both at the periphery and in the central regions of cells (Figures 3A and 3B). No

externalization of septins was observed in platelets upon activation assessed by the absence of the Septin-2 and Septin-9 immunofluorescence in non-permeabilized resting and activated platelets (Figure S8). Quantification of the colocalization between Septin-2 or Septin-9 and α-tubulin (in terms of cell volume averaged PCC) revealed that thrombin-induced platelet activation was followed by a significant 10% reduction of the average PCC values for both types of septins associated with α-tubulin (Figure 3C). In addition, the average degree of spatial overlap of α-tubulin with Septin-2 and with Septin-9 (expressed as Manders' colocalization coefficients, MCC) in thrombin-activated platelets was significantly reduced compared to resting platelets (Figure S2B). The reduction of the degree of colocalization between septins and α-tubulin upon platelet activation suggests diminished association between the cytoskeletal proteins.

Changes in cellular distribution of septins in resting and activated platelets induced by the septin inhibitor forchlorfenuron (FCF)

To elucidate further the role of septins in platelet structure and dynamics, isolated resting platelets were incubated for 40 min with a septin inhibitor, FCF, known to impair septin assembly, organization, and dynamics without affecting actin or tubulin polymerization/depolymerization and structure (Hu et al., 2008). In resting platelets, treatment with FCF caused dramatic alterations in the cellular organization of Septin-2 and Septin-9 and in their colocalization with tubulin (Figure 4). First, treatment of resting platelets with a relatively low concentration of FCF (25 μM) triggered partial reorganization of the Septin-2 peripheral ring revealed as a significant 20% increase of the mean ring thickness (Figures 4A and 4B). Second, treatment of resting platelets with a higher FCF concentration (50 μM) induced partial or complete disruption of the Septin-2 ring and formation of elongated Septin-2, -9 structures (Figure 4A). Third, the 50 μM FCF treatment of resting platelets resulted in a significant 1.7- and 3.4-fold reduction in the mean fluorescence intensity of Septin-2 and Septin-9, respectively, suggesting disassembly of septin supramolecular structures, such as the marginal band and clusters of Septin-2 and Septin-9 in the central part of cells (Figure 4C).

Lastly, in resting platelets, FCF induced differential changes in the colocalization of Septin-2 and Septin-9 with α-tubulin, quantified in terms of the platelet volume-averaged Pearson's correlation coefficients (Figure 4D) and Mander's colocalization coefficients (Figure S9). In particular, there was an insignificant decrease of the mean $PCC^{SPT2/\alpha T}$ value at $\leq$50 μM FCF with respect to untreated cells, implying that FCF did not alter the relation between Septin-2 and α-tubulin fluorophore intensities. At the same time, the average $PCC^{SPT9/\alpha T}$ value was significantly reduced by 20% at 50 μM FCF compared to untreated platelets, suggesting that the association between Septin-9 and α-tubulin was weaker than that for Septin-2 and α-tubulin. It is noteworthy that changes in the extent of spatial overlap in terms of Mander's coefficients for both Septin-2/α-tubulin and Septin-9/α-tubulin were more sensitive to variations of FCF than PCC values (Complementary results, Analysis of co-occurrence between Septin-2,9 and α-tubulin for resting and activated platelets in the presence of FCF, Figure S9). In particular, the extent of the overlap between Septin-2 and α-tubulin in resting platelets revealed significant changes at 50 μM FCF, while a decrease in the overlap between Septin-9 and α-tubulin was distinct at the lower concentration of FCF (25 μM) (Figure S9). These findings suggest that the septin inhibitor FCF induces disruption of the septin spatial organization in resting platelets accompanied by Septin-9 and tubulin structural rearrangements, leading to the reduction of the proteins' spatial overlap.

Pre-treatment of platelets with FCF had remarkable consequences for the cytoskeletal remodeling in response to platelet activation by thrombin, including changes in the densities of Septin-2 and Septin-9 and their colocalization with α-tubulin (Figure 5). In comparison to thrombin-activated cell without FCF, activated FCF-treated platelets showed a significant three- and 3.3-fold decrease in the average fluorescence intensity of Septin-2 and Septin-9, respectively, implying reduced compactness/density of septins in the presence of FCF (Figures 5A and 5B). The impairment of septin assembly in the presence of FCF caused a significant 16 and 10% decrease of the platelet volume-averaged $PCC^{SPT2/\alpha T}$ and $PCC^{SPT9/\alpha T}$ values, respectively, suggesting a weak association of the Septin-2, Septin-9 and α-tubulin in activated platelets in the presence of FCF. In addition, FCF caused a significant decrease of Mander's coefficients, indicating diminished spatial overlap between Septin-2, Septin-9 and α-tubulin (Figure S9). Noteworthy, the decrease in the $PCC^{SPT2/\alpha T}$ and $PCC^{SPT9/\alpha T}$ induced by FCF in thrombin-activated platelets was larger than in resting FCF-pre-treated resting or untreated thrombin-activated platelets, implying that the disruptive effects of thrombin and FCF on association between septins and tubulins are cumulative.

Thus, dysregulation of septin assembly with FCF resulted in reduced colocalization of septins and α-tubulin following platelet activation. Overall, septin perturbations by FCF resulted in significant alterations in the

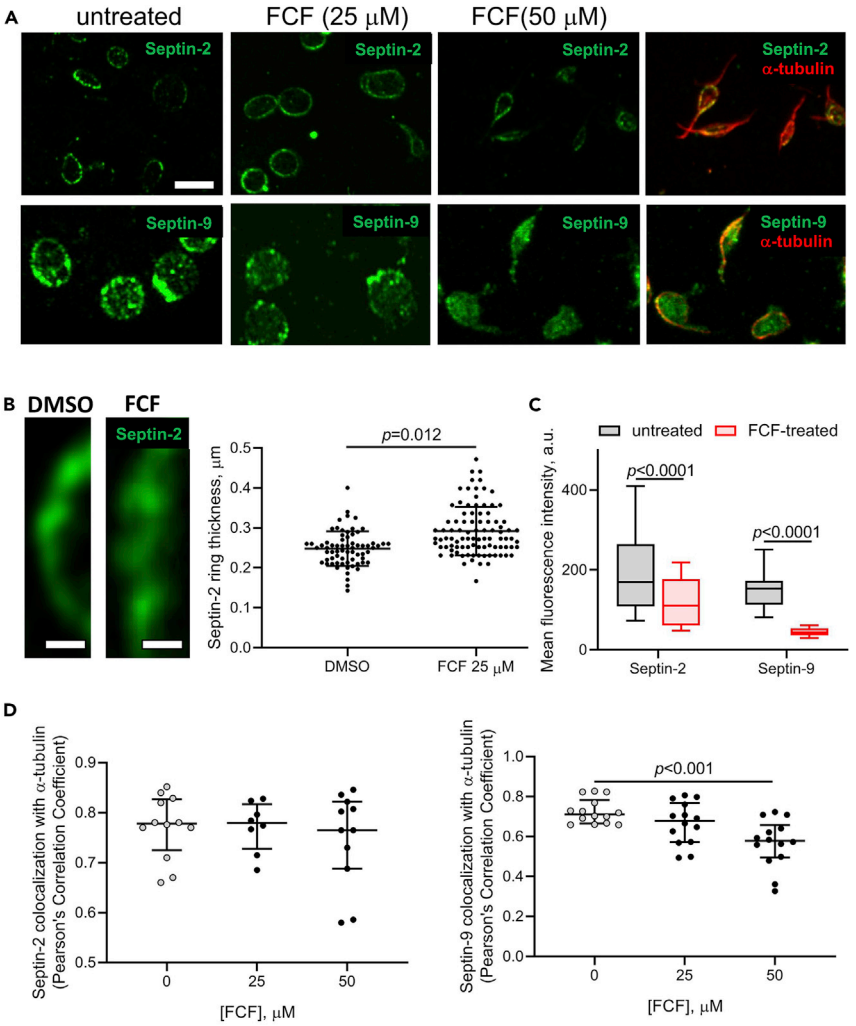

Figure 4. Structural rearrangements of Septin-2 and Septin-9 in resting platelets induced by FCF, the inhibitor of septin dynamics

(A) Representative immunofluorescence images of Septin-2, Septin-9 and α-tubulin in DMSO-treated (control) and FCF-treated resting platelets showing dose-dependent intraplatelet structural alterations by FCF. Scale bar = 3 μm. Projections of optical z stack slices.

(B) FCF-induced changes in the thickness of Septin-2-ring-like circular structures: (left) a segment of the Septin-2 ring in the absence and presence of FCF; (right) quantification of the Septin-2 ring thickness in untreated and FCF-treated platelets (n > 70, Mean ± SD). Scale bar = 0.4 μm. Significance tested by the two-tailed Mann-Whitney U test.

(C) Mean fluorescence intensity of Septin-2 and Septin-9 in the absence (n = 110 cells) and presence (n = 110) of 50 μM FCF measured at the identical settings of a confocal fluorescent microscope. The results are presented as a median and IQR. Significance tested by the Mann-Whitney.

(D) FCF-induced changes in the correlation of fluorescence intensity (Pearson) between Septin-2 and α-tubulin (D, left) and Septin-9 and α-tubulin (D, right), showing reduction of the spatial overlap between septins and α-tubulin in the presence of FCF. Data are presented as a median and IQR. Significance tested by the Kruskal-Wallis test with post hoc Dunn's correction for multiple comparisons. Data in (C and D) are presented as a median and IQR.

spatial intracellular organization of Septin-2 and Septin-9 and their colocalization with α-tubulin in both resting and thrombin-activated platelets.

Changes in morphology of platelets induced by forchlorfenuron (FCF)

Confocal microscopy imaging of FCF-treated and untreated resting platelets revealed that disruption of septin assembly caused dramatic morphological changes in platelets (Figures 6A, 6B, and S10). Qualitatively, at the FCF concentrations larger than 25 μM platelets lost their discoid shape and became

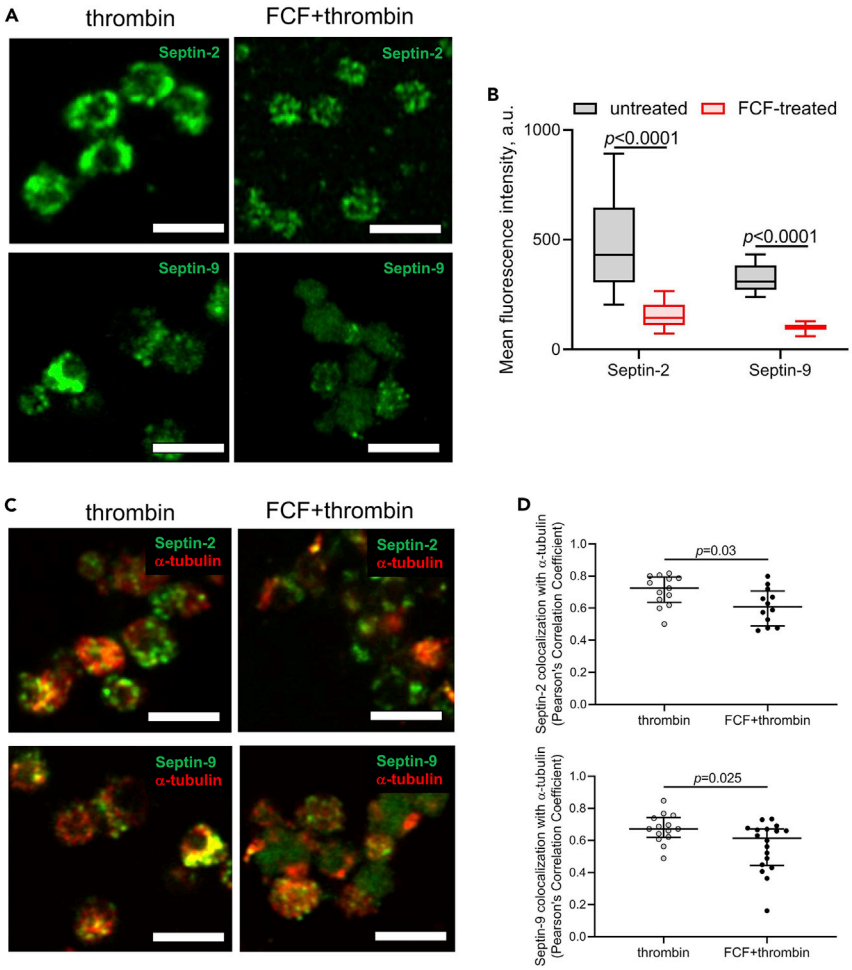

Figure 5. Structural alterations induced by a septin inhibitor FCF in thrombin-activated platelets

(A) Immunofluorescence confocal microscopy of Septin-2 and Septin-9 in thrombin-activated platelets in the absence and presence of 50 μM of FCF showing decrease of sepins compaction caused by FCF. Scale bar = 3 μm. Projections of optical z stack slices.

(B) Images in A quantified in terms of the mean fluorescence intensity measured at the identical settings of a confocal fluorescent microscope (n = 80 cells, Median and IQR).

(C) Immunofluorescence microscopy of Septin-2, Septin-9 and α-tubulin in thrombin-activated platelets in the absence and presence of 50 μM of FCF.

(D) FCF-induced changes in the fluorescence correlation (Pearson) between Septin-2 and α-tubulin (D, top) and Septin-9 and α-tubulin (D, bottom), displaying reduced spatial association between septins and tubulin. The results are presented as a median and IQR. Significance tested by the Mann-Whitney U-test.

elongated. A further increase of the FCF concentration (50 μM) resulted in emergence of thin, pseudopod-like structures from the opposite ends of the elongated cells. To quantify the platelet shape changes resulting from disturbed assembly of septins, we have calculated platelet roundness and solidity, the geometric parameters describing the extent of cell circularity and concavity, at different concentrations of FCF. Our data showed that the morphometric parameters characterizing the platelet shape depended on the FCF concentrations. Platelet roundness and solidity both significantly decreased on average by 16 and 16% at 25 μM FCF and by 28 and 24%, respectively, at 50 μM FCF in comparison to FCF-untreated platelets (Figures 6C and 6D). These observations suggest that septins play a structural role by supporting the platelet curved discoid shape. Of note, our results demonstrate that inhibition of septin assembly by FCF in thrombin-activated platelets can promote and accelerate platelet fragmentation, suggesting contribution of septins in maintaining platelet integrity (Complementary results, Impairment of platelet-driven clot contraction induced by FCF, Figure S11).

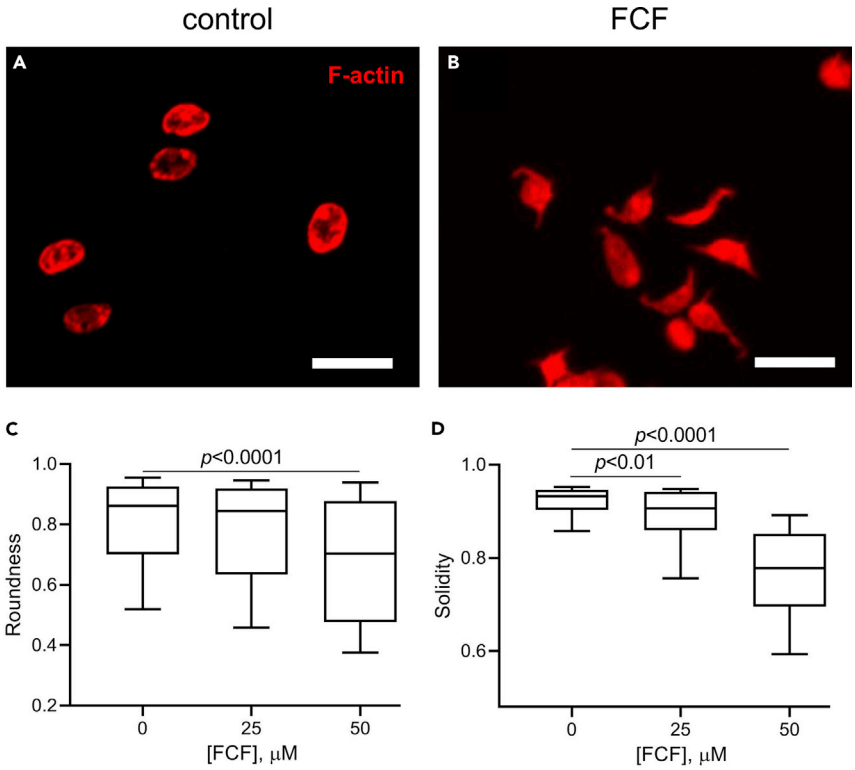

Figure 6. Changes in resting platelet morphology associated with septin perturbations induced by FCF

(A and B)Representative confocal microscopy images of DMSO-treated control resting platelets (A) and platelets treated with 50 μM FCF (B). Scale bar = 5 μm. Projections of optical z stack slices.

(C and D) Morphometry of FCF-treated resting platelets in terms of platelet roundness (C) and solidity (D) at various FCF concentrations (n = 100, Median and IQR). Gel-filtered platelets were incubated with various FCF concentration for 40 min, followed by fixation, staining for F-actin and imaging. Significance tested by the Kruskal-Wallis test with post hoc Dunn's correction for multiple comparisons.

Effects of septin perturbation on platelet functionality

FCF-induced changes in the surface expression of platelet activation markers

To assess the impact of septin perturbations on the surface expression of the markers of platelet activation (P-selectin, phosphatidylserines, and active integrin αIIbβ3), we performed flow cytometry of resting and TRAP-activated isolated platelets in the absence and presence of FCF (Figure 7). In resting platelets exposed to 50 μM FCF, there was a significant 2.6-fold increase of the average P-selectin expression level, in comparison to the FCF-untreated platelets (Figure 7A). At the same time, FCF treatment did not affect the exposure of phosphatidylserines in resting platelets (Figure 7B). In addition, the surface expression of active αIIbβ3 as well as the overall αIIbβ3 (active and non-active conformations) were unaltered in resting platelets treated with 50 μM FCF (Figures 7C and S12). These findings show that in resting platelets FCF at 50 μM increases the P-selectin expression without concomitant αIIbβ3 integrin activation and phosphatidylserine exposure, suggesting that septin disruption by FCF promotes secretion of α-granules, the depot of P-selectin.

In contrast to FCF-treated resting platelets, in TRAP-activated platelets pre-treated with 25 μM or 50 μM FCF the phosphatidylserine exposure increased significantly compared to the activated cells not treated with FCF (Figure 7B). At the same time, thrombin-induced integrin αIIbβ3 activation was significantly reduced, on average 2-fold, at 50 μM FCF in comparison to activated control FCF-untreated platelets (Figure 7C), with the overall integrin αIIbβ3 expression being unaltered by FCF (Figure S12), suggesting reduced integrin-ligand binding affinity for platelets with inhibited septin assembly. Notably, FCF caused no significant changes in the expression of P-selectin in TRAP-activated platelets (Figure 7A).

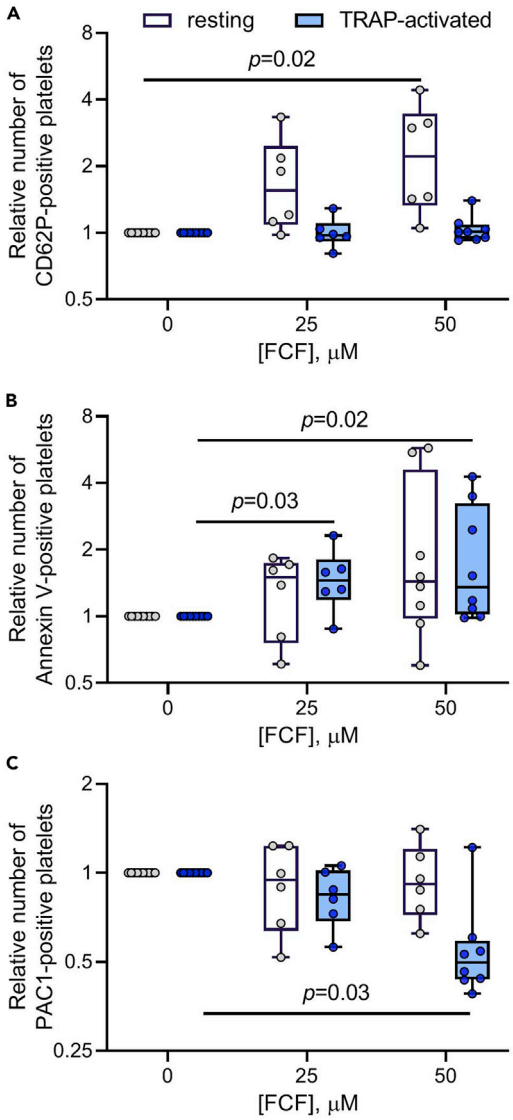

Figure 7. Effects of FCF on the expression of molecular markers of activation in resting and TRAP-activated platelets detected using flow cytometry

(A) Ratios of the fractions of P-selectin-expressing (CD62-positive) platelets in the presence of FCF and in the absence of FCF (control) taken as 1.

(B) Ratios of the fractions of phosphatidylserine expressing (Annexin V-positive) platelets in the presence of FCF and in the absence of FCF (control) taken as 1.

(C) Ratios of the fractions of platelets expressing active αIIbβ3 (determined by PAC-1 binding) in the presence of FCF and in the absence of FCF (control) taken as 1.

Data are presented as a median and IQR. Significance tested by the Kruskal-Wallis test with post hoc Dunn's correction for multiple comparisons: significance is shown compared to DMSO-treated control platelets.

Remarkably, the observed alterations in platelet surface marker expression occurred in the absence of noticeable changes in the intercellular ATP content (Figure S13), indicating that FCF-induced inhibition of septin assembly did not alter platelet energy metabolism.

Overall, the impairment of septin dynamics in resting and activated platelets caused significant changes in the surface expression of the markers of platelet activation, including an increase of P-selectin-expression on resting platelets, an increase of phosphatidylserine exposure on activated platelets, and reduced expression of the active αIIbβ3 integrin on activated platelets.

Defective spreading of platelets caused by FCF

To explore if damping of septin dynamics affects spreading of human platelets, we used confocal microscopy to compare untreated and FCF-treated isolated platelets spread on a fibrinogen-coated surface (Figure 8A). Characterization of individual platelets in terms of their area in the spread state and the percentage exhibiting stress fibers indicated remarkable differences between FCF-treated and untreated platelets (Figure 8B). Specifically, in the presence of 50 μM FCF, the average area of spread platelets (STAR Methods, section confocal microscopy image analysis) was significantly reduced by 56% and there were 32% fewer individual platelets, in which stress fibers were detected, when compared to the FCF-untreated platelets. Spreading of untreated platelets was accompanied by disassembly of the Septin-2 ring, while in FCF-treated platelets the Septin-2-containing subcortical ring was prevented from disruption (Figure 8C). In addition to the continuous peripheral rings, in spread platelets three additional Septin-2-containing structures were identified, namely: discontinuous peripheral rings, filamentous structures, and fluorescent puncta stained for Septin-2 (Figure 8C). The majority of untreated platelets contained the puncta (30% of the total number of untreated cells) and filamentous structures (62%) built of Septin-2. In contrast, the dominant fraction of FCF-treated platelets contained partially disrupted Septin-2 rings (45% of the total number of treated cells) and filamentous Septin-2 structures (30%) (Figure 8D). Overall, inhibition of septin dynamics with FCF prevented full spreading of platelets on a fibrinogen-coated surface, suggesting that septin assembly and disassembly play a role in cytoskeletal rearrangements underlying the surface spreading of human platelets.

Impairment of platelet-driven clot contraction induced by FCF

To study the impact of septin dynamics on platelet contractility assessed via the platelet-driven contraction of blood clots, platelet-rich-plasma (PRP) clots were formed in the absence (control) and presence of FCF and the temporal changes in the clot size, fibrin network density, and contractile stresses were measured as described in STAR Methods (sections kinetics of clot contraction, fluorescent staining of isolated platelets for septins, F-actin, α-tubulin, βIIbβ3 integrin and membrane, platelet spreading). First, we tracked the size changes of PRP clots over time using serial clot images acquired by the Thrombodynamics Analyzer System (Figure 9A). Analysis of kinetic curves of the contracting PRP clots revealed that FCF caused a dose-dependent delay of the onset of clot contraction as shown by a significant 2.5- and 6.6-fold increase of the mean contraction lag time at 25 and 50 μM FCF, respectively (Figure 9B). Furthermore, both the mean extent of clot contraction and the average velocity of clot contraction both decreased significantly, 1.5- and 10-fold in the presence of 25 μM or 50 μM FCF, respectively, when compared to control clots. Next, analysis of the fibrin network structural alterations using z-stack images collected over the course of clot contraction with a confocal microscope revealed a significant 1.2-fold average decrease of fibrin densification in PRP clots in the presence of 50 μM FCF (Figures 9C and 9D). Finally, measurements of the contractile stress generated by platelets in the PRP clots formed between two parallel plates of the rheometer (see STAR Methods, section fluorescent staining of isolated platelets for septins, F-actin, α-tubulin, βIIbβ3 integrin and membrane), showed a substantial 6-fold reduction of the mean contractile stress in the presence of 50 μM FCF (Figure 9E). Taken together, the results indicate that FCF-induced impairment of the assembly of platelet septins results in a significant reduction of platelet-induced volumetric shrinkage and densification of PRP clots as well as a decrease of the contractile stress generated by activated platelets. These findings suggest that septin reorganization plays a significant role in the generation of traction forces and mechanotransduction in platelets during contraction of blood clots.

Complementary results

Analysis of colocalization between Septin-2 and Septin-9 in resting platelets

Analysis of z stack confocal microscopy images of Septin-2 and Septin-9 in resting platelets show a moderate colocalization of Septin-2 and Septin-9 (Pearson's coefficient = 0.54) averaged over an individual cell volume (Figure S1). The average Mander's coefficients calculated for Septin-2 and Septin-9, characterizing their fractional overlap, were about ~0.5–0.6 mainly because of the septins overlap at the platelet periphery. In summary, the colocalization analysis suggests a weak interaction between Septin-2 and Septin-9 in human platelets.

Analysis of co-occurrence between Septin-2,9 and α-tubulin for resting and activated platelets

In resting platelets, the average $MCC_{MB}^{SPT2/\alpha T} = 0.89$, $MCC_{MB}^{SPT9/\alpha T} = 0.74$ (Figure S2A). In contrast with the peripheral location, Septin-2 and Septin-9 in the central part revealed significantly lower spatial

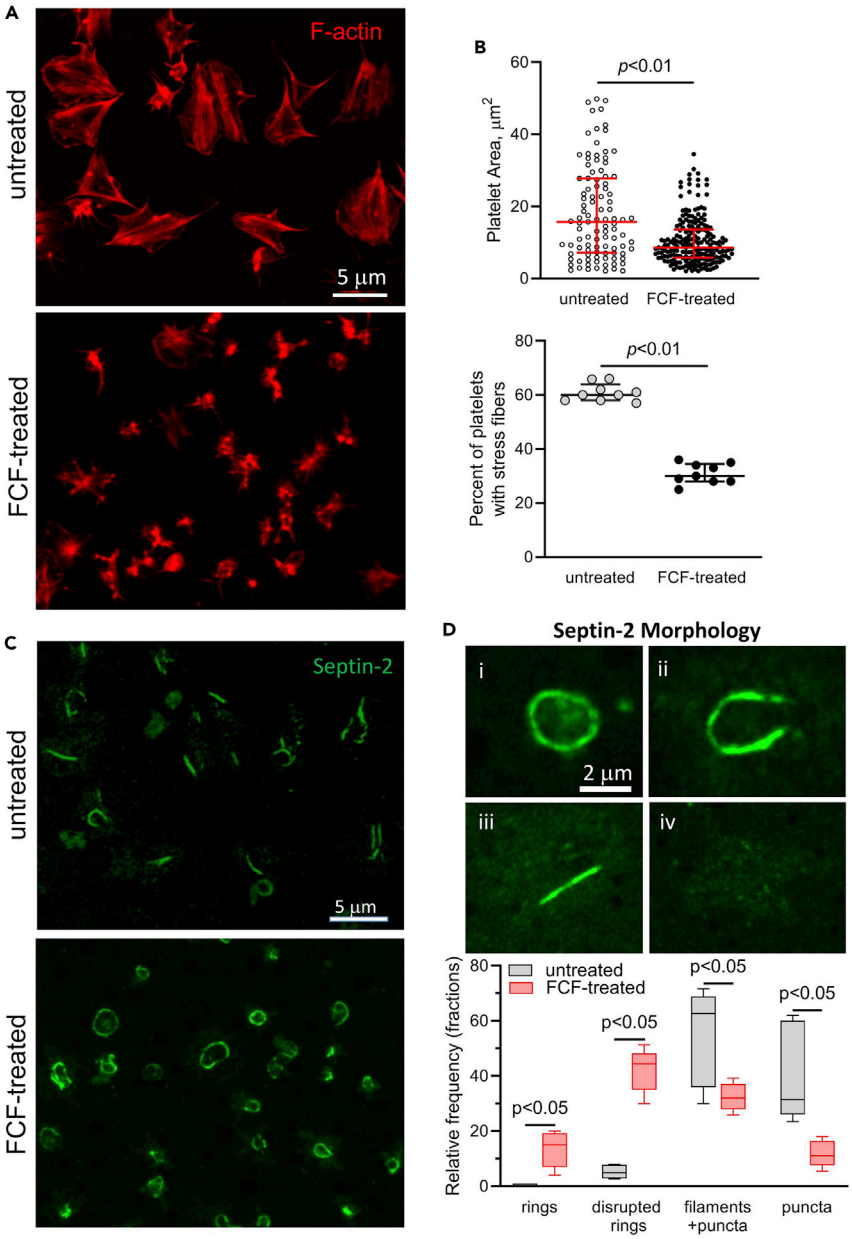

Figure 8. Abrogation of platelet spreading and supramolecular structural alterations of Septin-2 induced by FCF in spread platelets

(A) Gel-filtered platelets spread on a fibrinogen-coated surface for 60 min, followed by fixation and staining for Septin-2 and F-actin. The images are the projections of optical z stack slices.

(B) The degree of platelet spreading in the absence and presence of FCF (50 µM) were quantified in terms of the spread area per platelet. The effect of septin dynamics inhibition on formation of stress fibers in spread platelets was evaluated by calculating the fraction of platelets having stress fibers in the presence and absence of FCF (n > 100 cells, Median and IQR). Significance tested by two-tail Mann-Whitney.

(C) Representative confocal microscopy images of Septin-2 in isolated platelets spread on fibrinogen for 60 min in the absence and presence of FCF, 50 µM.

(D) Four types of Septin-2 structures identified in spread platelets: continuous subcortical rings (i), partially discontinued rings (ii), filamentous structures surrounded by fluorescent puncta (iii), single puncta stained for Septin-2 (iv). Quantification of Septin-2 structures in spread platelets in the absence and presence of FCF in terms of the relative frequency of Septin-2 structures defined in (i-iv). n = 50–80 cells per sample, N = 3 donors, Median and IQR. Significance tested by two-tail Mann-Whitney.

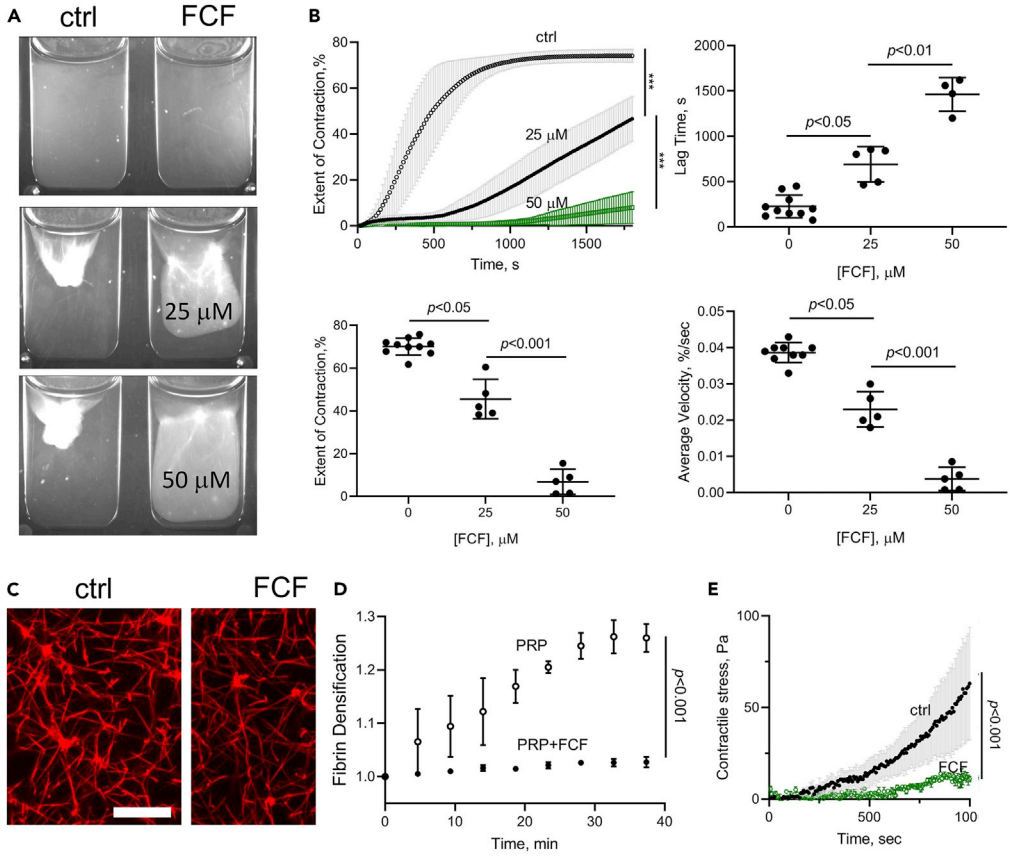

Figure 9. Impaired platelet-driven plasma clot contraction in the presence of FCF

(A) Photographic images of contracted platelet-rich-plasma clots in the absence and presence of FCF. Control (left) and FCF-treated (right) PRP clots before (A top) and after (A middle, bottom) contraction at 25 and 50 μM of FCF (final concentration) after 30 min of pre-incubation. Clotting was induced by 1 U/mL thrombin and 26 mM $CaCl_2$ followed by the optical tracking clot contraction.

(B) Quantification of clot contraction at various concentrations of FCF. Averaged kinetic curves of clot contraction for PRP with and without FCF (B top, left). Parameters of clot contraction (Mean ± SD, n = 5–10): the lag time (B top, right), the extent of contraction (B bottom, left), the average velocity of contraction (B bottom, right). Significance tested by Kolmogorov-Smirnov (B top, left) and Kruskal-Wallis test with post hoc Dunn's correction for multiple comparisons; significance shown with respect to control with DMSO (B top right, B bottom).(C and D) Reduced platelet-induced densification of fibrin in the absence and presence of FCF during clot contraction. PRP samples were preincubated without or with 50 μM FCF.

(C) Representative fluorescence confocal microscopy images of fibrin networks for a control PRP clot and PRP clot with FCF after 40-min incubation. Projections of optical 10-μm thick z stack slices. Scale bar = 15 μm.

(D) Temporal changes of fibrin network densification assessed in terms of its fluorescence intensity relative to fibrin fluorescence in the uncontracted clot at t = 0 (Mean ± SD, n = 4).

(E) Temporal changes in platelet contractility in the absence and presence of 50 μM FCF. Significance tested by Kolmogorov-Smirnov test. PRP samples were preincubated without or with 50 μM FCF. Clots were formed between parallel plates of a rheometer and the contractile (normal) force on the movable upper plate was measured (Mean ± SD, n = 3). Clotting was induced with 1 U/mL thrombin and 26 mM $CaCl_2$.

overlap with α-tubulin when compared to peripheral MB region: average $MCC_{Central}^{SPT2/\alpha T}$ = 0.53, $MCC_{Central}^{\alpha T/SPT9}$ = 0.47. In addition, MCC values averaged over the entire platelet space indicated that the fraction of Septin-2 overlapping with α-tubulin is about 23% higher than that of Septin-9 ($MCC^{SPT2/\alpha T}$ = 0.85 vs $MCC^{\alpha T/SPT2}$ = 0.69, $p < 0.01$, Mann-Whitney U-test).

In thrombin-activated platelets, the average degree of spatial overlap of α-tubulin with Septin-2 and with Septin-9 (expressed as Manders' coefficients, MCC) was reduced by 21 and 30%, respectively, compared to resting platelets (Figure S2B). Yet, thrombin-induced platelet activation did not change the relative amount of Septin-2 and Septin-9 overlapped with α-tubulin as revealed by the corresponding MCC values.

Analysis of co-occurrence between Septin-2,9 and α-tubulin for resting and activated platelets in the presence of FCF

In resting platelets (Figures S3A and S3B), MCCs for Septin-2 and α-tubulin indicated a significant increase in the average fraction of Septin-2 overlapped with α-tubulin and a decrease in the fraction of α-tubulin overlapped with Septin-2 at 50 μM FCF. The latter suggests that disruption of Septin-2 structures in resting platelets induced by FCF was spatially nonuniform, such that the α-tubulin-associated fraction of the platelet Septin-2 diminished (disassembled) slower than the fraction of Septin-2 not overlapping with α-tubulin. In contrast to Septin-2, the influence of low FCF concentration (25 μM) on the overlap between Septin-9 and α-tubulin in resting platelets was significant. Specifically, calculations of $MCC^{SPT9/\alpha T}$ and $MCC^{\alpha T/SPT9}$ indicated a 19 and 42% average decrease in the fraction of Septin-9 overlapping with α-tubulin and the fraction of α-tubulin overlapping with Septin-9, respectively. Furthermore, treatment of platelets with 50 μM of FCF significantly reduced the average $MCC^{SPT9/\alpha T}$ value by 43%, which, when compared to the decrease in $MCC^{SPT2/\alpha T}$ by 14%, suggests that the spatial relation between Septin-9 and α-tubulin is more sensitive to septin assembly disruption than the relation between Septin-2 and α-tubulin.

In thrombin-activated FCF-treated platelets (Figure S2C), $MCC^{SPT2/\alpha T}$ and $MCC^{SPT9/\alpha T}$ were lower than in untreated activated cells on average by 19 and 11%, respectively at 50 μM FCF.

Impact of septin inhibition on platelet fragmentation

It was shown previously that thrombin-activated platelets in about 1 h and later after activation become dysfunctional and undergo fragmentation (Kim et al., 2019). To examine if septins play a role in the fragmentation of platelets, we monitored, in parallel, the fate of FCF-untreated and FCF-treated thrombin-activated platelets in PRP clots over the time course of 100 min, using a confocal microscope. Assessment of platelet fragmentation dynamics in the absence and presence of FCF (in terms of the fraction of fragmented platelets) revealed that in the presence of 50 μM FCF, thrombin-activated FCF-treated platelets started to disintegrate about 15 min earlier than thrombin-activated FCF-untreated platelets. Accordingly, the average extent of platelet fragmentation in PRP clots after 100 min of incubation was 1.6-times higher than in the FCF-untreated clots. These results show that inhibition of septin assembly by FCF in thrombin-activated platelets can promote and accelerate platelet fragmentation.

Effects of the septin inhibitor, FCF, on platelet aggregation

Light transmission aggregometry (Chrono-log 700, PA, USA) of activated human platelets in PRP was performed in the presence and absence of the septin inhibitor, FCF. We found that pre-treatment of platelets with 50 μM FCF for 1hat 37 °C in PRP, significantly impaired platelet aggregation induced by 5 μM or 20 μM of TRAP-6. 20 μM TRAP-6 induced irreversible platelet aggregation of both untreated and FCF-treated platelets (Figure S16). Inhibition of septin dynamics with FCF in platelets stimulated with 20 μM TRAP-6 reduced the maximum extent of platelet aggregation and the rate of aggregation by 8 and 21%, respectively, compared to non-treated platelets. 5 μM TRAP-6 induced reversible aggregation of both untreated and FCF-treated platelets (Figure S16). FCF reduced the maximum degree of platelet aggregation 3.4-fold and decreased the rate of aggregation by 33%, compared to untreated platelets stimulated with 5 μM TRAP6. Therefore, our findings suggest that septin dynamics support aggregation of platelets.

DISCUSSION

In nucleated mammalian cells, septins assemble into filaments and higher order structures that are involved in a variety of cellular processes, including cytokinesis, cytoskeletal rearrangements, membrane remodeling, and secretion (Bridges and Gladfelter, 2015; Gilden et al., 2012; Kartmann and Roth, 2001). Although septins have been detected in platelets, very little is known about the role of septins in platelet biology including participation of septins in platelet cytoskeletal remodeling upon activation and platelet functionality. Meanwhile, platelet cytoskeleton dynamics underlies platelet shape changes and is involved in multiple platelet functions such as adhesion, secretion, spreading, and contractility (Zaninetti et al., 2020). Therefore, it is important to delineate the contribution of the septin cytoskeleton to platelet structure and function. We studied resting and activated human platelets and revealed differential distributions of Septin-2 and Septin-9 within the platelet volume. We found that septin assembly and disassembly play an important role in maintaining platelet shape and is critical for platelet functions, including contractility, spreading, and responses to activating stimuli. The aggregate of the results obtained in this study and their biological implications are condensed in Table 1.

Septin-2 and -9 (re)arrangements and association with microtubules in resting and activated platelets

Previous studies revealed that septins associate with other cytoskeletal components, including microtubules (Bridges and Gladfelter, 2015; Lam and Calvo, 2019). Moreover, Septin-5 and Septin-6 were found to be structurally and functionally associated with the microtubular network and to co-localize with the cortical tubulin ring in platelets (Martinez et al., 2006). Similarly, the preferential circumferential arrangements of Septin-2 and -9 and their localization with tubulin has been revealed in our work (Figure 2), suggesting that septins may be engaged together with microtubules in providing shape stability of resting platelets. The interaction between septins and tubulins could be mediated by MAP4, microtubule motors or other linkers (Kremer et al., 2005; Spiliotis, 2010). Another possible mechanism, underlying the peripheral arrangement of Septin-2 and Septin-9 can be related to the interactions between polybasic domains of septins and negatively charged phosphoinositides of the inner leaflet of the plasma membrane (Song et al., 2016). Accumulation of septins in platelet subcortical regions with largest curvature is in agreement with the fact that septins can recognize micrometer-scale curvature in the absence of other cellular factors, resembling septin distributions in mammalian cells of different types (Beber et al., 2019; Bridges et al., 2016; Cannon et al., 2019).

Formation of condensed septin structures in thrombin-activated platelets (Figure 3) suggests septin clusterization, polymerization, and/or otherwise induced densification. It is likely that the observed septin densification in activated platelets is a result of myosin-driven contraction and compaction of the actin network, leading to concentration of cytoplasmic proteins, including septins. The increased immunofluorescent signal in thrombin-stimulated platelets may result also from the enhanced *de novo* synthesis of septins regulated by platelet microRNAs, such as mir223-3p (Lazar et al., 2020), followed by polymerization of newly formed septins. Indeed, our results indicate a significant increase in Septin-2 protein expression following platelet activation (Figure S6). The above-mentioned possibilities, i.e., the cytoskeletal shrinkage and/or septin expression, are not mutually exclusive and can work in concert.

Another structural feature of septins in the activated platelets is that the colocalization between septins and α-tubulin is reduced (Figure 3), suggesting that septins and tubulin fall apart or dissociate. It is tempting to speculate that septins partially dissociate from the microtubular networks for the sake of a higher structural flexibility of the plasma membrane in activated platelets required for platelet morphological changes such as formation of dynamic filopodia and lamellipodia (Ageta-Ishihara et al., 2013; Dolat et al., 2014b; Hu et al., 2012; Tada et al., 2007). Although the interplay between septins and microtubules is not clear, septins may be involved in the dynamics of the microtubule ring, needed for platelet shape changes (Diagouraga et al., 2014). Indeed, dysregulation of septin assembly with FCF results in marked rearrangements of Septin-2 and Septin-9 in both resting and activated platelets, accompanied by microtubules disorganization (Figures 4 and S14). In contrast to the tight band that microtubules form in untreated resting platelets, in FCF-treated platelets, microtubules displayed separated concentric loops with microtubule ends diverging from the circumferential orientation (Figure S14), suggesting that septins organize and maintain the dynamics of circumferential microtubules in resting platelets. In fact, oligomeric complexes of septins 2/6/7 were shown to directly promote microtubule formation by enhancing microtubule growth and elongation whereas septins in a polymeric state inhibited microtubule growth (Nakos et al., 2019).

Forchlorfenuron (FCF) as a tool to study platelet septins

Forchlorfenuron (FCF), a septin inhibitor, has been broadly used to study septins inside various cell types (Hu et al., 2008; Iwase et al., 2004; Tokhtaeva et al., 2015; Vardi-Oknin et al., 2013; Zhang et al., 2016). FCF is a plant cytokinin previously shown to disrupt septin localization in budding yeast (Iwase et al., 2004). *In silico* studies have revealed that FCF interacts primarily with the nucleotide-binding pockets of septins (Angelis et al., 2014). FCF was suggested to interact with the P loop Walker A motif GxxxxGKS/T, binding the phosphatase of GTP, and the GTP specificity motif AKAD, interacting with the guanine base of GTP and threonine, which is critical for GTP hydrolysis. Thus, the current working model for FCF suggest that FCF stabilizes septins by preventing GTP binding and hydrolysis.

Although the specificity of FCF toward septins was questioned (Sun et al., 2019), still there has been good evidence for the usefulness of applying FCF as a pharmacological tool to study structural and physiological roles of septins in mammalian cells (Deb et al., 2016; Hu et al., 2008; Møller et al., 2018; Sharma et al., 2013; Sidhaye et al., 2011). In particular, the effects of FCF on exocytosis, mitosis, cell migration and adhesion are similar to those induced by knockdown of specific septins using siRNA (Hu et al., 2008; Sidhaye et al., 2011).

At relatively low concentrations (<100 μM) FCF has been shown to specifically alter septin organization in mammalian cells and, again, the effects of FCF on cells are similar to those observed when the septin genes are silenced (Tokhtaeva et al., 2015). Platelets lack nuclei, but contain all essential cytoskeletal components including septins, therefore representing a cellular system in which off-target effects of FCF are minimized. It is noteworthy that in our experiments with human platelets FCF was applied at low concentrations (≤50 μM) to exclude non-specific effects of the FCF on other cytoskeletal elements (Hu et al., 2008). Importantly, we observed no difference in the intracellular ATP content of platelets untreated and treated with FCF (Figure S13), which makes the non-specific cytotoxic effect of FCF unlikely, at least at the experimental conditions applied.

Septin cytoskeleton contributes to the platelet morphology

Our results provide evidence that septins contributing to platelet cytoskeletal deformability, enhancing their structural stability. Surprisingly, the FCF-induced morphological changes in resting platelets (Figure 6) resemble those observed in spherical HeLa cells, in which FCF also induced cell elongation (Hu et al., 2008), implying that defects in cellular morphology caused by septin destabilization do not depend on the presence of a nucleus. Localization of septins at the platelet periphery suggests that the septin scaffold enhances cortical stiffness and membrane structure similar to that of nucleated cells, such in T-cells or mouse spermatozoa (Ihara et al., 2005; Tooley et al., 2009). In addition, septins presumably stabilize the cell cortex through their interactions with actomyosin complexes and the plasma membrane in platelets as in other cell types (Gilden et al., 2012). Reduction in cortical stiffness can also partially explain accelerated fragmentation of activated platelets (Figure S11), revealing the role of septins in supporting structural integrity of activated platelets.

Septins mediate surface expression of platelet activation markers (P-selectin, phosphatidylserines, and the active integrin αIIbβ3)

Examination of surface activation markers in platelets with FCF-inhibited septin assembly revealed the role of septins in various mechanisms of platelet activation. One such mechanism is the release of platelet granules via exocytosis reflected by increased P-selectin expression in resting platelets (Figure 7). Meanwhile, in activated platelets, the impact of FCF on P-selectin exposure has not been observed, most-likely due to the strong platelet activation effect induced by TRAP, which resulted in a large fraction of CD62p-positive platelets (72 ± 18%), preventing detection of changes caused by FCF (Figure S15). Since P-selectin is known to be located in platelet α-granules, structural rearrangements caused by septin disturbances might enhance α-granule transport and release of contents at the platelet surface, therefore suggesting a role for septin assembly in platelet secretion. This finding is in general agreement with previous studies, suggesting involvement of Septin-5 and Septin-8 in mouse platelet granule release (Dent et al., 2002; Neubauer et al., 2021). In particular, platelets in Septin5-knockout mice facilitated secretion of serotonin at subthreshold levels of collagen-induced platelet activation (Dent et al., 2002). Septin8-knock out in mice caused a defect in α-granule but not in δ-granule and lysosomal secretion (Neubauer et al., 2021), suggesting that different septins may cause different secretion defects. It is noteworthy that both FCF and knockdown of Septin-2 inhibited constitutive and stimulated exocytosis in various cell types (Tokhtaeva et al., 2015).

Another mechanism of platelet activation is increased procoagulant activity in thrombin-activated platelets reflected by an increase in PS exposure (Figure 7). Septin hexamers can directly bind to PS through electrostatic interactions (Szuba et al., 2021), suggesting that septin alterations may cause direct translocation of PS at the absence of septin externalization (Figure S8). Perhaps, septin-driven membrane remodeling indirectly affects the phospholipid flip-flopping catalyzed by flippases (Lhermusier et al., 2011). Flippase activity could be modulated by a septin-associated kinase, such as Gin4 in yeast, which therefore may contribute to asymmetric distribution of PS (Roelants et al., 2015). Interestingly, deletion of Septin8 in mice reduces PS exposure in convulxin-treated platelets (Neubauer et al., 2021), whichsupports our findings of septin participation in exposure of procoagulant PS.

At the same time, the reduced expression of the activated integrin on treatment of platelets with FCF suggests that septin assembly is required for surface expression and/or activation of the integrin to make platelets more adhesive and prone to aggregation (Figure S16). In fact, Septin-8 deletion in mice has been shown to reduce activation of αIIbβ3, along with a decrease in platelet adhesion and aggregation (Neubauer et al., 2021). Possibly, integrin activation is indirectly affected by septins: expression of Septin-9_i1 was shown to positively correlate with paxillin (Zeng et al., 2019), forming a complex with kindlin and talin needed to support αIIbβ3 activation (Gao et al., 2017). Yet, the regulatory mechanism of how

septins potentiate integrin activation requires further elucidation. Reduction of active integrin expression in platelets with perturbed septin dynamics can partially explain the defective spreading of platelets on a fibrinogen-coated surface (Figure 8). A previous study has shown that platelet spreading strongly and positively correlates with platelet PAC-1 binding, the degree of active integrin exposure on the platelet surface (Hosseini et al., 2019), supporting the fact that the lack of αIIbβ3-fibrinogen binding can result in an underdeveloped lamellipodia. These results are also in agreement with a recent study, indicating that deletion of Septin-8 in mouse caused a pronounced defect in integrin activation and significant reduction in platelet spreading (Neubauer et al., 2021). Another potential role of septins in platelet spreading might be their functional interdependence with actin; in particular, Septin-2 was shown to stabilize actin stress fibers, preventing actin turnover, and therefore contributing to lamellipodia formation (Schmidt and Nichols, 2004). Of interest, septin structures can undergo disintegration upon platelet spreading (Figure 8). The fact that septins provide membranes with stiffness and structural stability suggests that septin remodeling might be required for platelets to fully spread. Interestingly, Martinez et al., 2006, observed ring-like structures formed by Septin-5 in platelets spread for 20 min whereas in our study the Septin-2 ring, presumably forming complex with a Septin-5, became dismantled after 40 min, indicating that remodeling of septin ring-like structures in spread platelets requires longer than a 20 min incubation period.

Septins modulate platelet contractility

The inhibited septin assembly in platelets was associated with significantly impaired contraction of platelet-rich plasma clots (Figure 9), suggesting septins' participation in the generation and/or transmission of platelet contractile force to fibrin. Based on the previous studies (Joo et al., 2007; Kinoshita et al., 2002), septins may affect contractility of platelets through direct interaction with non-myosin IIA (Joo et al., 2007) and also via anillin binding to F-actin (Kinoshita et al., 2002). On the other hand, mechanotransduction mediated via αIIbβ3-fibrin(ogen) binding (Hansen et al., 2018) can be compromised in the presence of FCF because of the reduced expression of active αIIbβ3 on the surface of activated platelets with perturbed septins (Figure 7C). Hence, septin-mediated platelet mechanics, including contraction of blood clots, may be another link between septins and platelet physiology.

Conclusions

Septin-2 and Septin-9 localize at the periphery of human resting platelets where they demonstrate strong association with microtubules. Thrombin-induced platelet activation caused condensation of Septin-2 and Septin-9 into clusters and reduced their colocalization with α-tubulin. Damping of septin assembly with FCF resulted in significant alterations of spatial intracellular organization of Septin-2 and Septin-9 and colocalization with α-tubulin in both resting and activated platelets. Septin assembly provides stability of the discoid shape of resting platelets. Impairment of septin dynamics increased phosphatidylserine exposure on activated platelets and P-selectin expression on resting platelets, as well as reduced expression of active αIIbβ3 integrin on activated platelets. Septin assembly plays an important role in supporting platelet biomechanical functions including spreading and contraction. In summary, our findings provide important insights into the role of septins in human platelet biology.

Limitations of the study

Detailed molecular mechanisms of interactions between septins and microtubules and other cytoskeletal components, as well as the role of individual septins in human platelet biology are not considered in the current work and warrant further investigation. Application of FCF and its limitations have been discussed in the Discussion *Section* above. Our findings provide strong evidence for the role of septins in platelet biology; however, further *in vivo* studies are needed to address the pathophysiological relevance of septins.

STAR★METHODS

Detailed methods are provided in the online version of this paper and include the following:

- KEY RESOURCES TABLE
- RESOURCE AVAILABILITY
  - Lead contact
  - Materials availability
  - Data and code availability
- EXPERIMENTAL MODEL AND SUBJECT DETAILS

SUPPLEMENTAL INFORMATION

Supplemental information can be found online at https://doi.org/10.1016/j.isci.2022.104654.

ACKNOWLEDGMENTS

The work was supported by American Heart Association grant 17SDG33680177(O.V.K.), National Institutes of Health grants R21DE030294 (O.V.K.), R01HL146373 (J.W.W., R.I.L), HL148227 (J.W.W., R.I.L) and GM116876(E.B.), University of Pennsylvania Bridge Grant, and the Strategic Academic Leadership Program (Priority-2030) at the Kazan Federal University (E.R.M.). We acknowledge the CDB Microscopy Core facility at the University of Pennsylvania for microscope use. We thank Kangji Wang for providing septin antibodies and staining protocol to collect preliminary data for this study.

AUTHOR CONTRIBUTIONS

Conceptualization, O.V.K., R.I.L., E.B., O.V., and J.W.W.; Data acquisition, O.V.K., E.R.M.; Formal Analysis, O.V.K.; Investigation, O.V.K., R.I.L., O.V., E.B.; Writing—Original Draft: O.V.K., R.I.L.; Writing—Review and Editing: all authors; Supervision and Project administration, J.W.W.

DECLARATION OF INTERESTS

The authors declare no competing interests.

Received: July 4, 2021
Revised: April 23, 2022
Accepted: June 17, 2022
Published: July 15, 2022

SUPPORTING CITATIONS

The following reference appears in the Supplemental Information: Bujold et al., 2016, Pontén et al., 2008.

REFERENCES

Aaron, J.S., Taylor, A.B., and Chew, T.-L. (2018). Image co-localization – co-occurrence versus correlation. J. Cell Sci. *131*, jcs211847. https://doi.org/10.1242/jcs.211847.

Ageta-Ishihara, N., Miyata, T., Ohshima, C., Watanabe, M., Sato, Y., Hamamura, Y., Higashiyama, T., Mazitschek, R., Bito, H., and Kinoshita, M. (2013). Septins promote dendrite and axon development by negatively regulating microtubule stability via HDAC6-mediated deacetylation. Nat. Commun. *4*, 2532. https://doi.org/10.1038/ncomms3532.

Angelis, D., Karasmanis, E.P., Bai, X., and Spiliotis, E.T. (2014). In silico docking of forchlorfenuron (FCF) to septins suggests that FCF interferes with GTP binding. PLoS One *9*, e96390. https://doi.org/10.1371/journal.pone.0096390.

Beber, A., Taveneau, C., Nania, M., Tsai, F.-C., Di Cicco, A., Bassereau, P., Lévy, D., Cabral, J.T., Isambert, H., Mangenot, S., and Bertin, A. (2019). Membrane reshaping by micrometric curvature sensitive septin filaments. Nat. Commun. *10*,

420. https://doi.org/10.1038/s41467-019-08344-5.

Beites, C.L., Peng, X.-R., and Trimble, W.S. (2001). 52 - expression and analysis of properties of septin CDCrel-1 in exocytosis. In Methods in Enzymology, Regulators and Effectors of Small GTPases, W.E. Balch, C.J. Der, and A. Hall, eds. (Academic Press), pp. 499–510. https://doi.org/10.1016/S0076-6879(01)29111-3.

Bennett, J.S., Hoxie, J.A., Leitman, S.F., Vilaire, G., and Cines, D.B. (1983). Inhibition of fibrinogen binding to stimulated human platelets by a monoclonal antibody. Proc. Natl. Acad. Sci. USA *80*, 2417–2421. https://doi.org/10.1073/pnas.80.9.2417.

Bläser, S., Horn, J., Würmell, P., Bauer, H., Strümpell, S., Nurden, P., Pagenstecher, A., Busse, A., Wunderle, D., Hainmann, I., and Zieger, B. (2004). The novel human platelet septin SEPT8 is an interaction partner of SEPT4. Thromb. Haemostasis *91*, 959–966. https://doi.org/10.1160/TH03-09-0578.

Bolte, S., and Cordelières, F.P. (2006). A guided tour into subcellular colocalization analysis in light microscopy. J. Microsc. *224*, 213–232. https://doi.org/10.1111/j.1365-2818.2006.01706.x.

Brass, L.F., Ma, P., Tomaiuolo, M., Diamond, S.L., and Stalker, T.J. (2017). A systems approach to the platelet signaling network and the hemostatic response to injury. In Platelets in Thrombotic and Non-Thrombotic Disorders (Springer), pp. 367–378.

Bridges, A.A., and Gladfelter, A.S. (2015). Septin form and function at the cell cortex. J. Biol. Chem. *290*, 17173–17180. https://doi.org/10.1074/jbc.r114.634444.

Bridges, A.A., Jentzsch, M.S., Oakes, P.W., Occhipinti, P., and Gladfelter, A.S. (2016). Micron-scale plasma membrane curvature is recognized by the septin cytoskeleton. J. Cell Biol. *213*, 23–32. https://doi.org/10.1083/jcb.201512029.

Bujold, D., Morais, D.A.D.L., Gauthier, C., Côté, C., Caron, M., Kwan, T., Chen, K.C., Laperle, J., Markovits, A.N., Pastinen, T., et al. (2016). The international human epigenome consortium data portal. Cell Syst. *3*, 496–499.e2. https://doi.org/10.1016/j.cels.2016.10.019.

Cannon, K.S., Woods, B.L., Crutchley, J.M., and Gladfelter, A.S. (2019). An amphipathic helix enables septins to sense micrometer-scale membrane curvature. J. Cell Biol. *218*, 1128–1137. https://doi.org/10.1083/jcb.201807211.

Cavini, I.A., Leonardo, D.A., Rosa, H.V.D., Castro, D.K.S.V., D'Muniz Pereira, H., Valadares, N.F., Araujo, A.P.U., and Garratt, R.C. (2021). The structural biology of septins and their filaments: an update. Front. Cell Dev. Biol. *9*, 765085. https://doi.org/10.3389/fcell.2021.765085.

Costes, S.V., Daelemans, D., Cho, E.H., Dobbin, Z., Pavlakis, G., and Lockett, S. (2004). Automatic and quantitative measurement of protein-protein colocalization in live cells. Biophys. J. *86*, 3993–4003. https://doi.org/10.1529/biophysj.103.038422.

Deb, B.K., Pathak, T., and Hasan, G. (2016). Store-independent modulation of Ca 2+ entry through orai by septin 7. Nat. Commun. *7*, 11751. https://doi.org/10.1038/ncomms11751.

Dent, J., Kato, K., Peng, X.-R., Martinez, C., Cattaneo, M., Poujol, C., Nurden, P., Nurden, A., Trimble, W.S., and Ware, J. (2002). A prototypic platelet septin and its participation in secretion. Proc. Natl. Acad. Sci. USA *99*, 3064–3069. https://doi.org/10.1073/pnas.052715199.

Diagouraga, B., Grichine, A., Fertin, A., Wang, J., Khochbin, S., and Sadoul, K. (2014). Motor-driven marginal band coiling promotes cell shape change during platelet activation. J. Cell Biol. *204*, 177–185. https://doi.org/10.1083/jcb.201306085.

Dolat, L., Hu, Q., and Spiliotis, E.T. (2014a). Septin functions in organ system physiology and pathology. Biol. Chem. *395*, 123–141. https://doi.org/10.1515/hsz-2013-0233.

Dolat, L., Hunyara, J.L., Bowen, J.R., Karasmanis, E.P., Elgawly, M., Galkin, V.E., and Spiliotis, E.T. (2014b). Septins promote stress fiber–mediated maturation of focal adhesions and renal epithelial motility. J. Cell Biol. *207*, 225–235. https://doi.org/10.1083/jcb.201405050.

El Amine, N., Kechad, A., Jananji, S., and Hickson, G.R.X. (2013). Opposing actions of septins and Sticky on Anillin promote the transition from contractile to midbody ring. J. Cell Biol. *203*, 487–504. https://doi.org/10.1083/jcb.201305053.

Evtugina, N.G., Peshkova, A.D., Pichugin, A.A., Weisel, J.W., and Litvinov, R.I. (2020). Impaired contraction of blood clots precedes and predicts postoperative venous thromboembolism. Sci. Rep. *10*, 18261. https://doi.org/10.1038/s41598-020-75234-y.

Frenette, P.S., Johnson, R.C., Hynes, R.O., and Wagner, D.D. (1995). Platelets roll on stimulated endothelium in vivo: an interaction mediated by endothelial P-selectin. Proc. Natl. Acad. Sci. USA *92*, 7450–7454. https://doi.org/10.1073/pnas.92.16.7450.

Gao, J., Huang, M., Lai, J., Mao, K., Sun, P., Cao, Z., Hu, Y., Zhang, Y., Schulte, M.L., Jin, C., et al. (2017). Kindlin supports platelet integrin αIIbβ3 activation by interacting with paxillin. J. Cell Sci. *130*, 3764–3775. https://doi.org/10.1242/jcs.205641.

Gilden, J.K., Peck, S., M Chen, Y.C., and Krummel, M.F. (2012). The septin cytoskeleton facilitates membrane retraction during motility and blebbing. J. Cell Biol. *196*, 103–114. https://doi.org/10.1083/jcb.201105127.

Hall, P.A., Jung, K., Hillan, K.J., and Russell, S.H. (2005). Expression profiling the human septin gene family. J. Pathol. *206*, 269–278. https://doi.org/10.1002/path.1789.

Hansen, C.E., Qiu, Y., McCarty, O.J.T., and Lam, W.A. (2018). Platelet mechanotransduction. Annu.Rev. Biomed. Eng. *20*, 253–275. https://doi.org/10.1146/annurev-bioeng-062117-121215.

Hosseini, E., Ghasemzadeh, M., Azizvakili, E., and Beshkar, P. (2019). Platelet spreading on fibrinogen matrix, a reliable and sensitive marker of platelet functional activity during storage. J. Thromb. Thrombolysis *48*, 430–438. https://doi.org/10.1007/s11239-019-01916-8.

Hu, J., Bai, X., Bowen, J.R., Dolat, L., Korobova, F., Yu, W., Baas, P.W., Svitkina, T., Gallo, G., and Spiliotis, E.T. (2012). Septin-driven coordination of actin and microtubule remodeling regulates the collateral branching of axons. Curr. Biol. *22*, 1109–1115. https://doi.org/10.1016/j.cub.2012.04.019.

Hu, Q., Nelson, W.J., and Spiliotis, E.T. (2008). Forchlorfenuron alters mammalian septin assembly, organization, and dynamics. J. Biol. Chem. *283*, 29563–29571. https://doi.org/10.1074/jbc.M804962200.

Ihara, M., Kinoshita, A., Yamada, S., Tanaka, H., Tanigaki, A., Kitano, A., Goto, M., Okubo, K., Nishiyama, H., Ogawa, O., et al. (2005). Cortical organization by the septin cytoskeleton is essential for structural and mechanical integrity of mammalian spermatozoa. Dev. Cell *8*, 343–352. https://doi.org/10.1016/j.devcel.2004.12.005.

Ivanov, A.I., Le, H.T., Naydenov, N.G., and Rieder, F. (2021). Novel functions of the septin cytoskeleton: shaping up tissue inflammation and fibrosis. Am. J. Pathol. *191*, 40–51. https://doi.org/10.1016/j.ajpath.2020.09.007.

Iwase, M., Okada, S., Oguchi, T., and Toh-e, A. (2004). Forchlorfenuron, a phenylurea cytokinin, disturbs septin organization in *Saccharomyces cerevisiae*. Genes Genet. Syst. *79*, 199–206. https://doi.org/10.1266/ggs.79.199.

Joo, E., Surka, M.C., and Trimble, W.S. (2007). Mammalian SEPT2 is required for scaffolding nonmuscle myosin II and its kinases. Dev. Cell *13*, 677–690. https://doi.org/10.1016/j.devcel.2007.09.001.

Junt, T., Schulze, H., Chen, Z., Massberg, S., Goerge, T., Krueger, A., Wagner, D.D., Graf, T., Joseph, E., Italiano, J., et al. (2007). Dynamic visualization of thrombopoiesis within bone marrow. Science *317*, 1767–1770. https://doi.org/10.1126/science.1146304.

Kartmann, B., and Roth, D. (2001). Novel roles for mammalian septins: from vesicle trafficking to oncogenesis. J. Cell Sci. *114*, 839–844. https://doi.org/10.1242/jcs.114.5.839.

Kim, M.-S., Pinto, S.M., Getnet, D., Nirujogi, R.S., Manda, S.S., Chaerkady, R., Madugundu, A.K., Kelkar, D.S., Isserlin, R., Jain, S., et al. (2014). A draft map of the human proteome. Nature *509*, 575–581. https://doi.org/10.1038/nature13302.

Kim, O.V., Litvinov, R.I., Alber, M.S., and Weisel, J.W. (2017). Quantitative structural mechanobiology of platelet-driven blood clot contraction. Nat. Commun. *8*, 1274–1284. https://doi.org/10.1038/s41467-017-00885-x.

Kim, O.V., Nevzorova, T.A., Mordakhanova, E.R., Ponomareva, A.A., Andrianova, I.A., Le Minh, G., Daminova, A.G., Peshkova, A.D., Alber, M.S., Vagin, O., et al. (2019). Fatal dysfunction and disintegration of thrombin-stimulated platelets. Haematologica *104*, 1866–1878. https://doi.org/10.3324/haematol.2018.202309.

Kinoshita, M. (2003). Assembly of mammalian septins. J. Biochem. *134*, 491–496. https://doi.org/10.1093/jb/mvg182.

Kinoshita, M., Field, C.M., Coughlin, M.L., Straight, A.F., and Mitchison, T.J. (2002). Self- and actin-templated assembly of Mammalian septins.

Dev. Cell *3*, 791–802. https://doi.org/10.1016/s1534-5807(02)00366-0.

Kremer, B.E., Haystead, T., and Macara, I.G. (2005). Mammalian septins regulate microtubule stability through interaction with the microtubule-binding protein MAP4. Mol. Biol. Cell *16*, 4648–4659. https://doi.org/10.1091/mbc.e05-03-0267.

Lam, M., and Calvo, F. (2019). Regulation of mechanotransduction: emerging roles for septins. Cytoskeleton *76*, 115–122. https://doi.org/10.1002/cm.21485.

Lazar, S., Wurtzel, J.G.T., Chen, X., Ma, P., and Goldfinger, L.E. (2020). High-efficiency unassisted transfection of platelets with naked double-stranded miRNAs modulates signal-activated translation and platelet function. Platelets *32*, 794–806. https://doi.org/10.1080/09537104.2020.1809642.

Le Minh, G., Peshkova, A.D., Andrianova, I.A., Sibgatullin, T.B., Maksudova, A.N., Weisel, J.W., and Litvinov, R.I. (2018). Impaired contraction of blood clots as a novel prothrombotic mechanism in systemic lupus erythematosus. Clin. Sci. *132*, 243–254. https://doi.org/10.1042/cs20171510.

Lefrançais, E., Ortiz-Muñoz, G., Caudrillier, A., Mallavia, B., Liu, F., Sayah, D.M., Thornton, E.E., Headley, M.B., David, T., Coughlin, S.R., et al. (2017). The lung is a site of platelet biogenesis and a reservoir for haematopoietic progenitors. Nature *544*, 105–109. https://doi.org/10.1038/nature21706.

Lhermusier, T., Chap, H., and Payrastre, B. (2011). Platelet membrane phospholipid asymmetry: from the characterization of a scramblase activity to the identification of an essential protein mutated in Scott syndrome. J. Thromb. Haemost. *9*, 1883–1891. https://doi.org/10.1111/j.1538-7836.2011.04478.x.

Longtine, M.S., DeMarini, D.J., Valencik, M.L., Al-Awar, O.S., Fares, H., De Virgilio, C., and Pringle, J.R. (1996). The septins: roles in cytokinesis and other processes. Curr.Opin. Cell Biol. *8*, 106–119. https://doi.org/10.1016/S0955-0674(96)80054-8.

Martinez, C., Corral, J., Dent, J.A., Sesma, L., Vicente, V., and Ware, J. (2006). Platelet septin complexes form rings and associate with the microtubular network. J. Thromb. Haemostasis *4*, 1388–1395. https://doi.org/10.1111/j.1538-7836.2006.01952.x.

Manders, E.M., Stap, J., Brakenhoff, G.J., van Driel, R., and Aten, J.A. (1992). Dynamics of three-dimensional replication patterns during the S-phase, analysed by double labelling of DNA and confocal microscopy. J. Cell Sci. *103*, 857–862. https://doi.org/10.1242/jcs.103.3.857.

Manders, E.M.M., Verbeek, F.J., and Aten, J.A. (1993). Measurement of co-localization of objects in dual-colour confocal images. J. Microsc. *169*, 375–382. https://doi.org/10.1111/j.1365-2818.1993.tb03313.x.

McMurray, M.A., and Thorner, J. (2019). Turning it inside out: the organization of human septin heterooligomers. Cytoskeleton *76*, 449–456. https://doi.org/10.1002/cm.21571.

Mendonça, D.C., Macedo, J.N., Guimarães, S.L., Barroso da Silva, F.L., Cassago, A., Garratt, R.C., Portugal, R.V., and Araujo, A.P.U. (2019). A revised order of subunits in mammalian septin complexes. Cytoskeleton *76*, 457–466. https://doi.org/10.1002/cm.21569.

Merten, M., and Thiagarajan, P. (2000). P-Selectin expression on platelets determines size and stability of platelet aggregates. Circulation *102*, 1931–1936. https://doi.org/10.1161/01.CIR.102.16.1931.

Møller, A.M.J., Füchtbauer, E.M., Brüel, A., Andersen, T.L., Borggaard, X.G., Pavlos, N.J., Thomsen, J.S., Pedersen, F.S., Delaisse, J.-M., and Søe, K. (2018). Septins are critical regulators of osteoclastic bone resorption. Sci. Rep. *8*, 13016. https://doi.org/10.1038/s41598-018-31159-1.

Monroe, D.M., Hoffman, M., and Roberts, H.R. (2002). Platelets and thrombin generation. Arterioscler.Thromb.Vasc. Biol. *22*, 1381–1389. https://doi.org/10.1161/01.ATV.0000031340.68494.34.

Mostowy, S., Bonazzi, M., Hamon, M.A., Tham, T.N., Mallet, A., Lelek, M., Gouin, E., Demangel, C., Brosch, R., Zimmer, C., et al. (2010). Entrapment of intracytosolic bacteria by septin cage-like structures. Cell Host Microbe *8*, 433–444. https://doi.org/10.1016/j.chom.2010.10.009.

Mostowy, S., and Cossart, P. (2012). Septins: the fourth component of the cytoskeleton. Nat. Rev. Mol. Cell Biol. *13*, 183.

Mostowy, S., Janel, S., Forestier, C., Roduit, C., Kasas, S., Pizarro-Cerdá, J., Cossart, P., and Lafont, F. (2011). A role for septins in the interaction between the Listeria monocytogenes invasion protein InlB and the Met receptor. Biophys. J. *100*, 1949–1959. https://doi.org/10.1016/j.bpj.2011.02.040.

Nakahira, M., Macedo, J.N.A., Seraphim, T.V., Cavalcante, N., Souza, T.A.C.B., Damalio, J.C.P., Reyes, L.F., Assmann, E.M., Alborghetti, M.R., Garratt, R.C., et al. (2010). A draft of the human septin interactome. PLoS One *5*, e13799. https://doi.org/10.1371/journal.pone.0013799.

Nakos, K., Radler, M.R., and Spiliotis, E.T. (2019). Septin 2/6/7 complexes tune microtubule plus-end growth and EB1 binding in a concentration- and filament-dependent manner. Mol. Biol. Cell *30*, 2913–2928. https://doi.org/10.1091/mbc.E19-07-0362.

Neubauer, K., Jurk, K., Petermann, V., Kumm, E., and Zieger, B. (2021). Impaired platelet function in Sept8-deficient mice in vitro. Thromb. Haemostasis *121*, 484–494. https://doi.org/10.1055/s-0040-1718733.

Oh, Y., and Bi, E. (2011). Septin structure and function in yeast and beyond. Trends Cell Biol. *21*, 141–148. https://doi.org/10.1016/j.tcb.2010.11.006.

Pagliuso, A., Tham, T.N., Stevens, J.K., Lagache, T., Persson, R., Salles, A., Olivo-Marin, J.-C., Oddos, S., Spang, A., Cossart, P., and Stavru, F. (2016). A role for septin 2 in Drp1-mediated mitochondrial fission. EMBO Rep. *17*, 858–873. https://doi.org/10.15252/embr.201541612.

Pinto, S.M., Manda, S.S., Kim, M.-S., Taylor, K., Selvan, L.D.N., Balakrishnan, L., Subbannayya, T., Yan, F., Prasad, T.S.K., Gowda, H., et al. (2014). Functional annotation of proteome encoded by human chromosome 22. J. Proteome Res. *13*, 2749–2760. https://doi.org/10.1021/pr401169d.

Pontén, F., Jirström, K., and Uhlen, M. (2008). The human protein atlas—a tool for pathology. J. Pathol. *216*, 387–393. https://doi.org/10.1002/path.2440.

Roelants, F.M., Su, B.M., von Wulffen, J., Ramachandran, S., Sartorel, E., Trott, A.E., and Thorner, J. (2015). Protein kinase Gin4 negatively regulates flippase function and controls plasma membrane asymmetry. J. Cell Biol. *208*, 299–311. https://doi.org/10.1083/jcb.201410076.

Rosen, E.D., Raymond, S., Zollman, A., Noria, F., Sandoval-Cooper, M., Shulman, A., Merz, J.L., and Castellino, F.J. (2001). Laser-induced noninvasive vascular injury models in mice generate platelet-and coagulation-dependent thrombi. Am. J. Pathol. *158*, 1613–1622. https://doi.org/10.1016/s0002-9440(10)64117-x.

Scharf, R.E. (2018). Platelet signaling in primary haemostasis and arterial thrombus formation: Part 2. Hämostaseologie *38*, 211–222. https://doi.org/10.1055/s-0038-1675149.

Schindelin, J., Arganda-Carreras, I., Frise, E., Kaynig, V., Longair, M., Pietzsch, T., Preibisch, S., Rueden, C., Saalfeld, S., Schmid, B., et al. (2012). Fiji: an open-source platform for biological-image analysis. Nat. Methods *9*, 676–682. https://doi.org/10.1038/nmeth.2019.

Schmidt, K., and Nichols, B.J. (2004). Functional interdependence between septin and actin cytoskeleton. BMC Cell Biol. *5*, 43. https://doi.org/10.1186/1471-2121-5-43.

Sharma, S., Quintana, A., Findlay, G.M., Mettlen, M., Baust, B., Jain, M., Nilsson, R., Rao, A., and Hogan, P.G. (2013). An siRNA screen for NFAT activation identifies septins as coordinators of store-operated Ca2+ entry. Nature *499*, 238–242. https://doi.org/10.1038/nature12229.

Shattil, S.J. (2005). Integrins and Src: dynamic duo of adhesion signaling. Trends Cell Biol. *15*, 399–403. https://doi.org/10.1016/j.tcb.2005.06.005.

Shattil, S.J. (1999). Signaling through platelet integrin αIIbβ3: inside-out, outside-in, and sideways. Thromb. Haemostasis *82*, 318–325. https://doi.org/10.1055/s-0037-1615849.

Sidhaye, V.K., Chau, E., Breysse, P.N., and King, L.S. (2011). Septin-2 mediates airway epithelial barrier function in physiologic and pathologic conditions. Am. J. Respir. Cell Mol. Biol. *45*, 120–126. https://doi.org/10.1165/rcmb.2010-0235OC.

Sirajuddin, M., Farkasovsky, M., Zent, E., and Wittinghofer, A. (2009). GTP-induced conformational changes in septins and implications for function. Proc. Natl. Acad. Sci. USA *106*, 16592–16597. https://doi.org/10.1073/pnas.0902858106.

Song, K., Russo, G., and Krauss, M. (2016). Septins as modulators of endo-lysosomal membrane traffic. Front. Cell Dev. Biol. *4*, 124. https://doi.org/10.3389/fcell.2016.00124.

Spiliotis, E.T. (2010). Regulation of microtubule organization and functions by septin GTPases.

Cytoskeleton *67*, 339–345. https://doi.org/10.1002/cm.20448.

Spiliotis, E.T., and Nelson, W.J. (2006). Here come the septins: novel polymers that coordinate intracellular functions and organization. J. Cell Sci. *119*, 4–10. https://doi.org/10.1242/jcs.02746.

Sun, J., Zheng, M.-Y., Li, Y.-W., and Zhang, S.-W. (2020). Structure and function of Septin 9 and its role in human malignant tumors. World J. Gastrointest.Oncol. *12*, 619–631. https://doi.org/10.4251/wjgo.v12.i6.619.

Sun, L., Cao, X., Lechuga, S., Feygin, A., Naydenov, N.G., and Ivanov, A.I. (2019). A Septin cytoskeleton-targeting small molecule, forchlorfenuron, inhibits epithelial migration via septin-independent perturbation of cellular signaling. Cells *9*, 84. https://doi.org/10.3390/cells9010084.

Szuba, A., Bano, F., Castro-Linares, G., Iv, F., Mavrakis, M., Richter, R.P., Bertin, A., and Koenderink, G.H. (2021). Membrane binding controls ordered self-assembly of animal septins. Elife *10*, e63349. https://doi.org/10.7554/eLife.63349.

Tada, T., Simonetta, A., Batterton, M., Kinoshita, M., Edbauer, D., and Sheng, M. (2007). Role of septin cytoskeleton in spine morphogenesis and dendrite development in neurons. Curr. Biol. *17*, 1752–1758. https://doi.org/10.1016/j.cub.2007.09.039.

Tokhtaeva, E., Capri, J., Marcus, E.A., Whitelegge, J.P., Khuzakhmetova, V., Bukharaeva, E., Deiss-Yehiely, N., Dada, L.A., Sachs, G., Fernandez-Salas, E., and Vagin, O. (2015). Septin dynamics are essential for exocytosis. J. Biol. Chem. *290*, 5280–5297. https://doi.org/10.1074/jbc.M114.616201.

Tooley, A.J., Gilden, J., Jacobelli, J., Beemiller, P., Trimble, W.S., Kinoshita, M., and Krummel, M.F. (2009). Amoeboid T lymphocytes require the septin cytoskeleton for cortical integrity and persistent motility. Nat. Cell Biol. *11*, 17–26. https://doi.org/10.1038/ncb1808.

Tutwiler, V., Peshkova, A.D., Andrianova, I.A., Khasanova, D.R., Weisel, J.W., and Litvinov, R.I. (2017). Contraction of blood clots is impaired in acute ischemic stroke. Arterioscler.Thromb.Vasc. Biol. *37*, 271–279. https://doi.org/10.1161/ATVBAHA.116.308622.

Trimble, W.S. (1999). Septins: a highly conserved family of membrane-associated GTPases with functions in cell division and beyond. J. Membr. Biol. *169*, 75–81. https://doi.org/10.1007/s002329900519.

Tutwiler, V., Litvinov, R.I., Lozhkin, A.P., Peshkova, A.D., Lebedeva, T., Ataullakhanov, F.I., Spiller, K.L., Cines, D.B., and Weisel, J.W. (2016). Kinetics and mechanics of clot contraction are governed by the molecular and cellular composition of the blood. Blood *127*, 149–159. https://doi.org/10.1182/blood-2015-05-647560.

Vardi-Oknin, D., Golan, M., and Mabjeesh, N.J. (2013). Forchlorfenuron disrupts SEPT9_i1 filaments and inhibits HIF-1. PLoS One *8*, e73179. https://doi.org/10.1371/journal.pone.0073179.

Verdier-Pinard, P., Salaun, D., Bouguenina, H., Shimada, S., Pophillat, M., Audebert, S., Agavnian, E., Coslet, S., Charafe-Jauffret, E., Tachibana, T., and Badache, A. (2017). Septin 9_i2 is downregulated in tumors, impairs cancer cell migration and alters subnuclear actin filaments. Sci. Rep. *7*, 44976. https://doi.org/10.1038/srep44976.

Weisel, J.W. (2007). Structure of fibrin: impact on clot stability. J. Thromb. Haemostasis *5*, 116–124. https://doi.org/10.1111/j.1538-7836.2007.02504.x.

Yokoyama, S., Ikeda, H., Haramaki, N., Yasukawa, H., Murohara, T., and Imaizumi, T. (2005). Platelet P-selectin plays an important role in arterial thrombogenesis by forming large stable platelet-leukocyte aggregates. J. Am. Coll. Cardiol. *45*, 1280–1286. https://doi.org/10.1016/j.jacc.2004.12.071.

Zaninetti, C., Sachs, L., and Palankar, R. (2020). Role of platelet cytoskeleton in platelet biomechanics: current and emerging methodologies and their potential relevance for the investigation of inherited platelet disorders. Hämostaseologie *40*, 337–347. https://doi.org/10.1055/a-1175-6783.

Zeng, Y., Cao, Y., Liu, L., Zhao, J., Zhang, T., Xiao, L., Jia, M., Tian, Q., Yu, H., Chen, S., and Cai, Y. (2019). SEPT9_i1 regulates human breast cancer cell motility through cytoskeletal and RhoA/FAK signaling pathway regulation. Cell Death Dis. *10*, 720. https://doi.org/10.1038/s41419-019-1947-9.

Zhang, N., Liu, L., Fan, N., Zhang, Q., Wang, W., Zheng, M., Ma, L., Li, Y., and Shi, L. (2016). The requirement of SEPT2 and SEPT7 for migration and invasion in human breast cancer via MEK/ERK activation. Oncotarget *7*, 61587–61600. https://doi.org/10.18632/oncotarget.11402.

Zuvanov, L., Mota, D.M.D., Araujo, A.P.U., and DeMarco, R. (2019). A blueprint of septin expression in human tissues. Funct. Integr. Genomics *19*, 787–797. https://doi.org/10.1007/s10142-019-00690-3.

STAR★METHODS

KEY RESOURCES TABLE

REAGENT or RESOURCE	SOURCE	IDENTIFIER
Antibodies		
Rabbit polyclonal antibodies against Septin-2	Invitrogen	Cat# PA5-53814; RRID: AB_2647124
Rabbit polyclonal antibodies against Septin-9	Novus Bio	Cat# NBP2-13294
Mouse monoclonal antibodies against human Septin-2	Proteintech	Cat# 60075-1-Ig
Mouse monoclonal anti-α-tubulin	Sigma-Aldrich	Cat# T6199; RRID: AB_477583
Anti-chicken α-tubulin antibodies	Sigma-Aldrich	Cat# T9026; RRID: AB_477593
Chicken Alexa Fluor 488-conjugated anti-rabbit-IgG antibodies	Invitrogen	Cat# A-21441; RRID: AB_2535859
Goat Alexa Fluor 568-conjugated anti-mouse-IgG antibodies	Invitrogen	Cat# A-11004; RRID: AB_2534072
Anti-human-CD62p PE-conjugated antibodies	Invitrogen	Cat# 304904; RRID: AB_314476
FITC-conjugated PAC-1 antibodies against activated human αIIbβ3	BD Biosciences	Cat# 340507; RRID: AB_2230769
Horseradish peroxidase-conjugated anti-rabbit IgG antibodies	SouthernBiotech	Cat# 4051-05; RRID: AB_2795965
Horseradish peroxidase-conjugated anti-mouse IgG antibodies	SouthernBiotech	Cat# 1036-05; RRID: AB_2794348
Monoclonal anti-human-αIIbβ3 integrin antibodies, A2A9, conjugated with Alexa Fluor 488	Dr. Bennett Lab, University of Pennsylvania; Bennett et al., (1983).	N/A
Chemicals, peptides, and recombinant proteins		
Sepharose CL-2B	Sigma-Aldrich	CAS# 65099-79-8
Thrombin from human blood plasma	Sigma-Aldrich	Cat# T4393
Thrombin receptor-activating peptide (TRAP-6)	Bachem Americas	Ref# 01-H-7764
Calcein AM	Molecular Probes	Cat# C3100MP, Lot# 1890561
Alexa Fluor 647-labeled human fibrinogen	Molecular Probes	Cat# F35200
FITC-labeled Annexin V	BioLegend	Cat# 640906
Phalloidin-iFluor 594	Abcam	Cat# Ab176757
Phosphate buffered saline (PBS)	Fisher Scientific	Cat# 10-010-072
Protease inhibitor cocktail	Sigma-Aldrich	Cat# P2714
Protein G- or A-coated magnetic beads	EMD Millipore	Cat# LSKMAGA02
HEPES	Sigma-Aldrich	Cat# H3375
Bovine serum albumin (BSA)	Sigma-Aldrich	Cat# A7030
Calcium chloride	Sigma-Aldrich	Cat# 383147
Magnesium chloride	Sigma-Aldrich	Cat# M8266
Potassium chloride	Fisher Scientific	Cat# BP366
Sodium chloride	Fisher Scientific	Cat# S271
Sodium phosphate	Fisher Scientific	Cat# S373
D-Glucose	Sigma-Aldrich	Cat# G8270
Ethylenediaminetetraacetic acid (EDTA)	Sigma-Aldrich	Cat# E-5134
Paraformaldehyde	Electron Microscopy Sciences	Cat# 15710
ECL Western Blotting Detection Reagents	Cytiva	Cat# RPN2209
Critical commercial assays		
4-12% NuPAGE Bis-Tris gels	Life Technologies	Ref# NP0335BOX
Nitrocellulose membranes	Life Technologies	Ref# IB301001
Software and algorithms		
Prism 8	GraphPad Prism	https://www.graphpad.com/

RESOURCE AVAILABILITY

Lead contact

Further information and requests for resources should be directed to the lead contact, Prof. John Weisel (weisel@pennmedicine.upenn.edu)

Materials availability

This study did not generate new unique reagents or resources.

Data and code availability

- All data reported in this paper will be shared by the lead contact on request.
- This paper does not report original code.
- Any additional information required to reanalyze the data reported in this paper is available from the lead contact on request.

EXPERIMENTAL MODEL AND SUBJECT DETAILS

Human blood samples

Blood was drawn by venipuncture from 30 healthy volunteers (Age: 18–45 years old, 15 males and 15 females) not taking any medications known to affect platelet function for at least 14 days. Written informed consent was obtained from the blood donors in accordance with a protocol approved by the University of Pennsylvania Institutional Review Board and in compliance with the Declaration of Helsinki. For experiments with platelet-rich plasma (PRP), whole blood stabilized with 3.2% trisodium citrate (9:1 v/v) was centrifuged at 210 g, 25°C, for 15 min immediately after blood withdrawal. The PRP was kept at room temperature and used within 4 h after blood collection.

METHOD DETAILS

Isolation and enumeration of platelets

Platelets were isolated from PRP at room temperature by gel-filtration on Sepharose CL-2B (Sigma-Aldrich, Sweden) equilibrated with modified Tyrode's buffer (5 mM HEPES, 134 mM NaCl, 3 mM KCl, 2 mM MgCl2, 5 mM D-glucose, 0.3 mM NaH2PO4, 1 mg/mL bovine serum albumin, Sigma A-7030, pH 7.4). Platelet count was performed in a ProCyte Dx Hematology Analyzer (IDEXX Lab Inc., Maine, US). Isolated platelets were used within 3 h after blood collection.

Activation of platelets by thrombin and formation of PRP-clots for confocal microscopy

Isolated untreated and FCF-treated platelets suspended in modified Tyrode's buffer were activated by adding human thrombin (Sigma-Aldrich, cat. #T4393, 1 U/mL final concentration) in the presence of 3 mM $CaCl_2$ and incubating for 15 min. Clotting of PRP and platelet activation were induced by adding human thrombin (1 U/mL final concentration) and $CaCl_2$ (26 mM final concentration). Immediately after activation, 30-μL PRP samples were quickly transferred onto 35 mm x 10 mm PELCO® clear wall glass bottom cell culture dishes and placed into the environmental chamber of the confocal microscope for real-time dynamic imaging of fluorescently labeled platelets and the fibrin network. Phosphate buffered saline (PBS) was added around the edge of a dish sealed with Parafilm to prevent sample evaporation.

Labeling of platelets and fibrin in PRP-clots for fluorescent confocal microscopy

PRP before activation with thrombin was spiked with fluorescent probes to visualize platelets and fibrin in a confocal microscope. Live platelets were labeled with calcein AM (Molecular Probes, Grand Island, NY, USA) at 0.2 μg/mL final concentration. Fibrin was visualized by adding Alexa Fluor 647-labeled human fibrinogen (Molecular Probes) at 40 μg/mL final concentration to PRP.

Confocal microscopy of fluorescently labeled PRP-clots

Clots freshly formed on a microscope cover slip were imaged in a Zeiss LSM880 laser scanning confocal microscope (Carl Zeiss MicroImaging GmbH, Germany) with Plan Apo 40x (NA 1.2) water immersion objective lens to obtain a series of high-resolution 212.5 μm × 212.5 μm x 20 μm z-stack images taken each 5 min during 40 min after clot formation. The distance between each z-stack slice was 0.6 μm with a resolution of 1024 × 1024 pixels; voxel size was 0.2076 × 0.2076 × 0.6896 μm^3. A combination of an argon laser beam

with a 488-nm wavelength and a helium-neon laser with a 633-nm wavelength was used to visualize both labeled platelets and fibrin at a time.

Measurement of contractile stress in PRP clots

To measure the dynamic bulk force induced by fibrin-attached activated platelets, a rheometer (ARG2; TA Instruments, New Castle, DE, USA) was used. Clots were formed in a 400-μm gap between a 20-mm flat parallel top plate and a fixed bottom plate of the rheometer by adding 1 U/mL thrombin and 26 mM $CaCl_2$ (final concentrations) to PRP. Force measurement started within 1 min after adding thrombin to PRP. The contractile stress was measured over time as a negative normal (vertical) force applied to the upper horizontal rheometer plate by the contracting clot divided by the contact surface area of the upper plate. To prevent sample drying at the clot-air interface, a thin layer of silicone oil was applied at the clot edge.

Kinetics of clot contraction

Clot size changes were tracked optically using a Thrombodynamics Analyzer System (HemaCore Ltd, Russia)(Tutwiler et al., 2016). Briefly, plasma clots were formed in plastic cuvettes, in which the walls were pre-lubricated with 4% v/v Triton X-100 in PBS to prevent fibrin sticking. Citrated PRP was recalcified with 26 mM $CaCl_2$ followed by addition of 1 U/mL thrombin (final) for initiation of clotting and clot contraction. 80-μL samples were transferred to transparent flat plastic cuvettes and imaged using a CCD camera. Changes in clot size were followed by acquiring images every 15 s for 30 min. Image sequence was analyzed computationally to plot contraction kinetic curves and measure the lag time, final extent of contraction, and average velocity.

Fluorescent staining of isolated platelets for septins, F-actin, α-tubulin, αIIbβ3 integrin and membrane

Isolated resting or thrombin-stimulated platelets (1×10^6 platelets in 100 μL of Tyrode's buffer) were fixed in suspension by 2% paraformaldehyde for 20 min. After three consequent washes in PBS, 12 min each, cells were permeabilized by incubation with 0.3% Triton X-100 for 5minat room temperature. Platelets were incubated in a blocking buffer (1% BSA, 0.3% Triton X-100 in PBS) for 60 min and stained. To evaluate possible externalization of septins on platelet activation, Triton X-100 was excluded from the blocking buffer to prevent membrane permeabilization. Double immunostaining for Septin-2 or -9 and α-tubulin was performed with rabbit polyclonal antibodies against Septin-2 (Invitrogen, PA5-53814, 1:50) or Septin-9 (Novus Bio, NBP2-13294, 1:150), and a mouse monoclonal anti-α-tubulin (Sigma, T6199, 1:500) antibody, respectively. Platelets were first incubated with primary antibodies diluted in the blocking buffer overnight at 4°C, washed with PBS followed by 90-min incubation with secondary Alexa Fluor 488-conjugated anti-rabbit antibodies (Invitrogen, A21441 1:1000) or Alexa Fluor 568-conjugated anti-mouse antibodies (Invitrogen, A-11004, 1:1000) at 37°C added simultaneously. To stain for F-actin, phalloidin-iFluor 594 (1:1000, Abcam) was added at the same time as the secondary antibody. To stain for the αIIbβ3 integrin, platelets were incubated with monoclonal anti-αIIbβ3 integrin antibodies, A2A9, conjugated with Alexa Fluor 488 (Bennett et al., 1983), at 4°C overnight. To fluorescently label platelet plasma membrane, fixed platelets were incubated with a lipophilic carbocyanine dye CellBrite Red, based on DiD (Biotium) for 15 min. Finally, platelets were washed in PBS three times for 12 min and attached to coverslip, mounted on glass slides.

Platelet spreading

Glass-bottom microwell dishes (MatTek) were coated with human fibrinogen (Sigma-Aldrich) in PBS (20 μg/mL) overnight at 4°C, then rinsed with PBS and air-dried. Gel-filtered platelets in Tyrode's buffer (pH 7.4) were layered onto fibrinogen-coated surfaces and platelets were allowed to spread for 60 min. For fluorescent microscopy, adherent platelets were fixed with 2% paraformaldehyde (PFA) for 20 min, permeabilized with 0.3% Triton X-100 in PBS for 5 min and washed 3 times with PBS. For fluorescent staining, platelets were incubated in the blocking buffer for 60minat a room temperature, followed by overnight incubation with primary antibodies against septin 2 (Invitrogen, PA5-53814, 1:50) at 4°C. Platelets were washed with PBS 3 times, 5 min each, followed by 90-min incubation at room temperature with secondary Alexa Fluor 488-conjugated anti-rabbit antibodies (Invitrogen, A21441 1:1000) and phalloidin-iFLuor 594 (1:1000, Abcam) added to each well with fixed platelets. Finally, platelets were washed in PBS three times for 5 min and imaged with a Zeiss LSM 880 microscope.

Confocal microscopy of isolated platelets

Fluorescent imaging *of* stained platelets was performed by confocal microscopy using an Airyscan mode of a Zeiss LSM 880 laser scanning confocal microscope with a 63×/1.4 oil-immersion objective lens. 66.5 μm × 66.5 μm × 4.2-μm z-stack images of platelets were acquired. The distance between adjacent slices was 0.16 μm and the voxel size of each image was 0.04 × 0.04 × 0.16 μm^3. 488-nm and 561-nm wavelength excitation laser lines were used.

Confocal microscopy image analysis

Analysis of acquired z-stack images of platelets was performed using standard plugins of Fiji software (Schindelin et al., 2012) to characterize platelet cytoskeletal alterations including changes in septin structure size, colocalization between septins and tubulin, and fluorescence intensity of septins. Measurements of platelet roundness and solidity parameters as well as spread platelet area were also performed in Fiji using standard functions. The area of spread platelets was assessed using z-projected images of platelets stained for F-actin. Confocal microscopy-based three-dimensional reconstruction of septin distribution was done in Imaris software (Imaris, Bitplane, USA).

The degree of septin compaction was assessed by the changes in the average septin fluorescence intensity and septin-occupied area per platelet on platelet activation. Fluorescence intensity of Septin-2 and Septin-9 in individual cells was measured in two ways. First, we determined the region of interest (ROI) for individual cells using standard ImageJ functions, "Threshold" and "Mask", followed by septin fluorescence intensity calculations in the defined ROIs. Second, the septin area per platelet was measured in the projections of optical z-stack slices of individual platelets. Using standard ImageJ functions, the 16-bit high-resolution images of platelet Septin-2 and Septin-9 were converted to binary images, followed by septin area calculations.

Protein colocalization analysis

To quantify the extent of intracellular colocalization of two fluorescent proteins in z-stack images of individual platelets, the Pearson's correlation coefficient (PCC), and Manders' colocalization coefficients (MCCs) were calculated, which characterize the fluorescence intensity correlation and co-occurrence (spatial overlap) of the two fluorophores, respectively (Manders et al., 1992, 1993). For an image comprising red and green fluorescent channels, the PCC values were calculated as $PCC = \frac{\sum_i (R_i - \overline{R})(G - \overline{G})}{\sqrt{(R_i - \overline{R})^2 \sum_i (G_i - \overline{G})^2}}$, where R_i and G_i refer to the intensity values for the *i*-th pixel, in the red and green channels, respectively; and $\overline{R}$ and $\overline{G}$ are the mean intensities of the red and green channels, respectively, across the entire image. The MCCs were defined as: $M_1 = \frac{\sum_i R_{i,coloc}}{\sum_i R_i}$, where $R_{i,coloc} = R_i$ for $G_i > 0$ and $R_{i,coloc} = 0$ for $G_i = 0$, $M_2 = \frac{\sum_i G_{i,coloc}}{\sum_i G_i}$, where $G_{i,coloc} = G_i$ for $R_i > 0$ and $G_{i,coloc} = 0$ for $R_i = 0$. ImageJ plugin JACoP was used for colocalization analysis of individual platelet z-stack images (Bolte and Cordelières, 2006).

Measurements of intracellular ATP content in platelets

Freshly isolated platelets (0.1mLat 10^7 cells/mL) in Tyrode's buffer were incubated for 30, 45, and 60 min without or with 50 μM thrombin receptor activated peptide (TRAP-6, Bachem Americas). Following incubation, platelets were spun down for 5minat 2,000 g and lysed with a lysis RIPA buffer (pH 7.4). Debris was removed from the lysates by centrifugation at 8,000 g for 10 min. ATP concentration in the platelet lysates was measured with a plate reader, Infinite 200 PRO (Tecan, Switzerland) using an ATP Bioluminescent Assay Kit (Sigma-Aldrich) according to the manufacturer's instructions.

Flow cytometry of isolated platelets

To assess expression of platelet activation markers, freshly isolated 200,000 platelets in 50 μL of Tyrode's buffer were incubated without or with TRAP-6 for 3 min. Platelets were centrifuged at 1,000 g for 5 min and re-suspended in 150 μL of a Ca^{2+}-containing buffer (10 mM HEPES, 140 mM NaCl, 2 mM $CaCl_2$, pH 7.4). The platelets were treated for 10minat room temperature in the dark with one of the following reagents: FITC-labeled Annexin V (BioLegend, USA), anti-CD62 PE-conjugated antibodies (Invitrogen, USA), or FITC-conjugated PAC-1 antibodies against activated αIIbβ3 (BD Biosciences, USA). Labeled platelet suspensions were diluted by the Ca^{2+}-containing buffer followed by flow cytometry. Platelets were gated in a flow cytometer by their forward scatter/side scatter (FSC/SCC) characteristics after size-based calibration with

1-, 2-, and 4-μm polystyrene beads. About 97% of events in the gate were CD41-positive (platelet-specific marker). For each sample analyzed, 30,000 events were collected using a FacsCalibur flow cytometer (BD Biosciences, USA) equipped with an argon laser (λ = 488 nm) and a diode red laser (λ = 635 nm). The data were analyzed using CellQuest Pro (BD Biosciences) and FlowJo software. At least six independently isolated platelet preparations were examined under each experimental condition.

Western blot analysis of Septin-2 expression in resting and activated platelets

Platelets were washed with 10 mM HEPES buffer, pH 6.5, containing 150 mM NaCl, 3 mM EDTA, 1M PGE1, and 0.3 units/mL apyrase. The washed platelets were re-suspended in modified Tyrode's buffer (see STAR Methods, Method details, section isolation and enumeration of platelets). Platelets were activated by incubation with 1 U/mL thrombin and 3 mM $CaCl_2$ for 15 min. Subsequently, five hundred-microliter aliquots of isolated washed resting and activated platelets ($2x10^8$ cells/mL) were lysed with 125 μL of 50 mM tris(hydroxymethyl)aminomethane (Tris) buffer containing 1% NP-40, 150 mM NaCl, 4 mM EDTA, and protease inhibitors (Protease Inhibitor Cocktail, Sigma-Aldrich). Proteins were then separated in 4-12% NuPAGE Bis-Tris gels (Life Technologies), and transferred to nitrocellulose membranes (IB301001, Life Technologies) for immunoblotting. Septin-2 was immunoblotted with the primary rabbit polyclonal antibodies against Septin-2 (Invitrogen, PA5-53814, 1:450). Immunoblotted protein bands were visualized using horseradish peroxidase-conjugated anti-rabbit IgG (SouthernBiotech, 4051-05, 1:1000) and ECL Western Blotting Detection Reagent (GE Healthcare Life Sciences).

Co-immunoprecipitation of Septin-2 with α-tubulin in resting and activated platelets

500 μL of isolated washed resting and activated platelets ($2x10^8$ cells/mL) were lysed with 125 μL of 50 mM tris(hydroxymethyl)aminomethane (Tris) buffer containing 1% NP-40, 150 mM NaCl, 4 mM EDTA, and protease inhibitors (Protease Inhibitor Cocktail, Sigma-Aldrich), centrifuged, and the supernatant was mixed with 10 μL of protein G- or A-coated magnetic beads (3322488, EMD Millipore, Germany) preincubated with mouse monoclonal anti-chicken α-tubulin antibodies (T9026, Sigma, 1:1000). After magnetic separation the products were eluted in a sample loading 2xSDS loading buffer from the beads for 5minat 70°C. Immunoprecipitates were subjected to electrophoresis onto 4–12% acrylamide gels (SDS-PAGE) and then transferred onto nitrocellulose (pore diameter 0.2 μm) membranes (Invitrogen). The presence of Septin-2 was detected by Western blot analysis. Septin-2 was immunoblotted with primary mouse monoclonal antibodies against Septin-2 (Proteintech, 60075-1-Ig, 1:20000). Immunoblotted protein bands were visualized using horseradish peroxidase-conjugated anti-mouse IgG (SouthernBiotech, 1036-05, 1:2000) and ECL Western Blotting Detection Reagent (GE Healthcare Life Sciences).

QUANTIFICATION AND STATISTICAL ANALYSIS

Statistical analysis was performed using a GraphPad Prism 8 software package. Statistical significance of the differences between paired groups or independent groups of samples were determined by a Wilcoxon matched-pairs signed rank test or a two-tail Mann-Whitney U test, respectively, with a 95% confidence level. The p value was calculated to establish the degree of significance. Statistical significance for multiple comparisons between more than two groups of independent variables was tested by the Kruskal-Wallis test with post-hoc Dunn's correction. Results are presented as a median and interquartile range (25th and 75th percentiles) unless otherwise indicated.